Avian eggshell formation reveals a new paradigm for vertebrate mineralization via vesicular amorphous calcium carbonate

Lilian Stapane, Nathalie Le Roy, Jacky Ezagal, Alejandro Rodriguez-Navarro, Valérie Labas, Lucie Combes-Soia, Maxwell Hincke, Joël Gautron

JBC ARTICLE

Avian eggshell formation reveals a new paradigm for vertebrate mineralization via vesicular amorphous calcium carbonate

Received for publication, July 20, 2020 Published, Papers in Press, August 18, 2020, DOI 10.1074/jbc.RA120.014542

Lilian Stapane[1], Nathalie Le Roy[1], Jacky Ezagal[1], Alejandro B. Rodriguez-Navarro[2], Valérie Labas[3], Lucie Combes-Soia[3], Maxwell T. Hincke[4], and Joël Gautron[1,*]

From [1]BOA INRAe, Université de Tours, Nouzilly, France, the [2]Departmento de Mineralogia y Petrologia, Universidad de Granada, Granada, Spain, the [3]Unité Mixte de Recherches Physiologie de la Reproduction et des Comportements, Université de Tours, IFCE, Nouzilly, France, and the [4]Department of Innovation in Medical Education, and Department of Cellular and Molecular Medicine, University of Ottawa, Ottawa, Canada

Edited by Gerald W. Hart

Amorphous calcium carbonate (ACC) is an unstable mineral phase, which is progressively transformed into aragonite or calcite in biomineralization of marine invertebrate shells or avian eggshells, respectively. We have previously proposed a model of vesicular transport to provide stabilized ACC in chicken uterine fluid where eggshell mineralization takes place. Herein, we report further experimental support for this model. We confirmed the presence of extracellular vesicles (EVs) using transmission EM and showed high levels of mRNA of vesicular markers in the oviduct segments where eggshell mineralization occurs. We also demonstrate that EVs contain ACC in uterine fluid using spectroscopic analysis. Moreover, proteomics and immunofluorescence confirmed the presence of major vesicular, mineralization-specific and eggshell matrix proteins in the uterus and in purified EVs. We propose a comprehensive role for EVs in eggshell mineralization, in which annexins transfer calcium into vesicles and carbonic anhydrase 4 catalyzes the formation of bicarbonate ions (HCO_3^-), for accumulation of ACC in vesicles. We hypothesize that ACC is stabilized by ovalbumin and/or lysozyme or additional vesicle proteins identified in this study. Finally, EDIL3 and MFGE8 are proposed to serve as guidance molecules to target EVs to the mineralization site. We therefore report for the first-time experimental evidence for the components of vesicular transport to supply ACC in a vertebrate model of biomineralization.

Biomineralization is a ubiquitous process by which living organisms produce minerals that they use for many different functions (*i.e.* protection, gravity sensing) (1). The formation of calcium carbonate ($CaCO_3$) or phosphate biominerals requires high local concentrations of calcium. Transient amorphous mineral phases that are highly soluble and reactive are a source of ions or a precursor phase for the formation of complex-shaped crystalline biomineral structures. Amorphous calcium carbonate (ACC) is a metastable polymorph of $CaCO_3$, and can provide high concentrations of ions for rapid physiological calcite and aragonite biomineralization (2). The high solubility of these metastable phases requires stabilization by regulatory molecules (3–9). Extracellular vesicles (EVs) are candidates to play a role in the stabilization and delivery of ACC (6–9). However, experimental evidence for EVs in ACC-mediated calcification in $CaCO_3$ biominerals is only available for invertebrate structures such as sea urchin spines (calcite) and molluscan shells (4, 10, 11).

Among vertebrates, the avian class (Aves) appeared around 91 million years ago and is divided into Paleognathae (ancient birds such as ostrich, rhea, and emu) and Neognathae (modern birds such as chicken, turkey, or zebra finch) (12). All birds produce eggs with a hard-mineral shell composed of $CaCO_3$ in the form of calcite, which is critical for development of the embryo within an autonomous chamber (13). In addition to defense against physical aggression, the eggshell protects the egg contents against microbial contamination, regulates water and gaseous exchange, and is a calcium source for embryonic bone calcification (14, 15). The chicken eggshell is a widely utilized experimental model for biomineralization. Eggshell formation occurs in the distal part of the hen oviduct (red isthmus and uterus) and is one of the fastest known processes of vertebrate biomineralization (16–18). In chickens, 6 g of $CaCO_3$ is rapidly deposited in a very short time (<18 h; deposition rate of 0.32 g/h) (19). During this extracellular process, the uterine cells secrete organic and mineral eggshell precursors into the uterine fluid (UF) where mineralization takes place (20–22). Both mineral and organic precursors interact to produce the specific eggshell texture and its resulting mechanical properties (17, 23). This process requires transport of large amounts of calcium and carbonate to the site of eggshell calcification; these ions are continuously supplied from the blood across the uterine epithelium (24). The active transepithelial transfer of calcium and carbonate is well described and constitutes the current model for eggshell calcification (21, 25). Alternatively, transport of stabilized ACC mineral in vesicles has been proposed (9).

In chicken eggshell mineralization, the important role of ACC has been described (26). During the earliest stage, massive deposits of ACC accumulate at specific nucleation sites (mammillary knobs) on the eggshell membrane. Subsequently, ACC transforms into calcite crystals. Moreover, progressive ACC dissolution continuously supplies local ions to support the

This article contains supporting information.

* For correspondence: Joël Gautron, joel.gautron@inrae.fr.

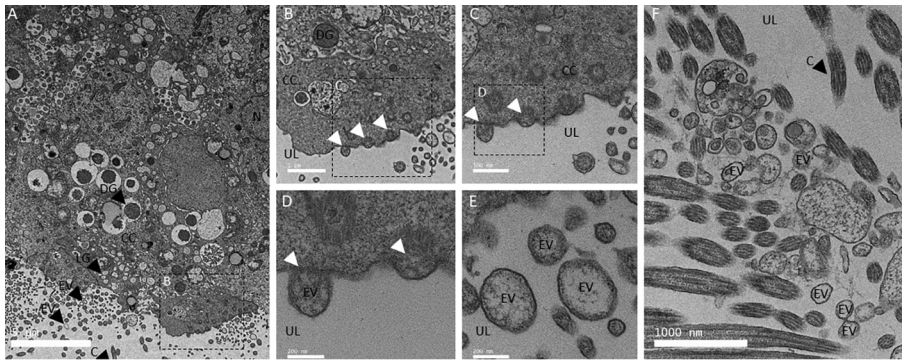

Figure 1. TEM of uterine cells. *A,* TEM micrograph of uterine epithelium showing secretory activity (16 h p.o.). *B–D,* higher magnification TEM micrographs of uterine cells showing examples of exocytosis activity. *E* and *F*, TEM micrographs illustrating the presence of numerous EVs in the uterine lumen (*UL*) at 7 (*F*) and 16 h p.o. (*E*). Thin sections of uterus were negatively stained with 2% uranyl acetate. *C,* cilia; *CC*, ciliated cells; *DG*, dense granule; *LG*, light granule; *N,* nucleus; *UL*, uterine lumen. *White arrowheads* indicate vesicle budding. *Bars*: *A* = 5 μM, *B* and *F* = 1000 nm, *C*= 500 nm, *D* and *E* = 200 nm.

rapid growth of columnar calcite crystals that constitute the palisade layer (26). In a recent study, we used bioinformatics tools, mRNA levels, and protein quantification to explore the role of EDIL3 and MFGE8 in chicken eggshell biomineralization. We hypothesized that EDIL3 and MFGE8 bind to EVs budding from uterine cells into the uterine fluid, to guide vesicular transport of stabilized ACC for delivery to the mineralizing site and moreover prevent nonspecific precipitation (27).

To test this hypothesis, in the current study we have used transmission EM (TEM) to investigate exocytosis activity at the apical plasma membrane of uterine cells that could be a source of EVs in the uterine fluid. We quantified mRNA levels of a variety of validated EV components in the oviduct segments and other tissues. We purified EVs from UF and demonstrated the presence of key vesicular proteins in these vesicles. Finally, spectroscopic techniques (energy-dispersive X-ray spectroscopy (EDX) and electron energy loss spectroscopy (EELS)) probed for ACC inside these EVs. This experimental study is the first to demonstrate vesicular transport of ACC in vertebrates, which we propose supports the rapid eggshell biomineralization process in birds.

Results

Transmission EM of uterine epithelial cells and uterine fluid

The presence of vesicles in the tissues and milieu involved in shell mineralization was investigated by TEM. Ultra-thin negatively stained sections of uterus epithelium were examined by TEM to investigate exocytosis activity adjacent to the luminal site of mineralization (Fig. 1). Uterine-ciliated cells possess numerous vacuolar and vesicular structures as well as dense and light granules (Fig. 1*A*). At higher magnification (Fig. 1, *B–D*) we observed vesicles in the cell cytoplasm, their accumulation at the apical plasma membrane, and their budding to generate EVs in the adjacent luminal uterine fluid (Fig. 1, *C* and *D*). Fig. 1, *E* and *F,* show EVs in the uterine fluid, with vesicle diameters in the 100-400 nm range. Vesicle membranes (rich in glycoproteins, proteins, and lipids) are stained by uranyl acetate and appear bright (high electron-density) *versus* their interiors that are darker (low electron density). However, some internal regions of vesicles also appeared electron-dense due to mineral deposits (see below). These TEM observations demonstrated the presence of vesicles in the luminal uterine fluid adjacent to the apical region of uterine cells. The uterine epithelium contains ciliated and nonciliated cells, and the same results were observed in proximity to nonciliated cells (data not shown). UF was also examined by TEM (Figs. 2 and 3), where numerous EVs varying in diameter from 100 to 500 nm were observed (Figs. 2, *A* and *C,* and 3*A*).

TEM and spectroscopic analysis of extracellular vesicle mineral deposits

At collection, uterine fluid was immediately frozen in liquid nitrogen to preserve EVs and their cargo. Uterine fluid vesicles containing electron dense mineral deposits were observed by TEM and analyzed by EELS (Fig. 2) and EDS (Fig. 3).

EELS spectra show characteristics peaks from the calcium $L_{2,3}$-edge (349.3 and 352.6 eV), carbon K-edge (285.0, 290.3, 295.5, and 301.5 eV), and oxygen K-edge (540.0 eV) (Fig. 2, *B* and *D*, Table S1). All carbon K-edge and oxygen K-edge peaks, except 285.0 eV, are characteristics of carbonate groups (28, 29). Thus, this analysis confirmed that the mineral deposits are calcium carbonate. Moreover, the 285.0 eV peak from the carbon K-edge is characteristic of amorphous carbon (from organics) and of C = C bonds, whereas the two peaks from the oxygen K-edge (534.0 and 545.5 eV) are also specific to C = O bonds (30). Therefore, EELS spectra confirmed the presence in the uterine EVs of an organic phase (phospholipids and proteins) as well as calcium carbonate mineral deposits, although low spectral resolution (0.25 eV) of the EELS detector did not allow differentiating among different polymorphs. However, selected area electron diffraction (SAED) of the vesicle mineral deposits showed diffuse rings indicative of the amorphous nature of calcium carbonate mineral (Fig. 3, *F* and *G*).

To determine the distribution of the organics and $CaCO_3$ mineral deposits, the carbon peak from the organics (237-290 eV) and calcium peaks (324-355 eV) were selected for mapping (Fig. 2, *E–H*). The carbon and calcium maps showed that the organic phase (C = C) was concentrated at the vesicle periphery (Fig. 2*G*), whereas calcium was concentrated within the vesicles. Merger of the carbon and calcium maps (Fig. 2*H*) clearly shows that the EV organic membranes (phospholipid

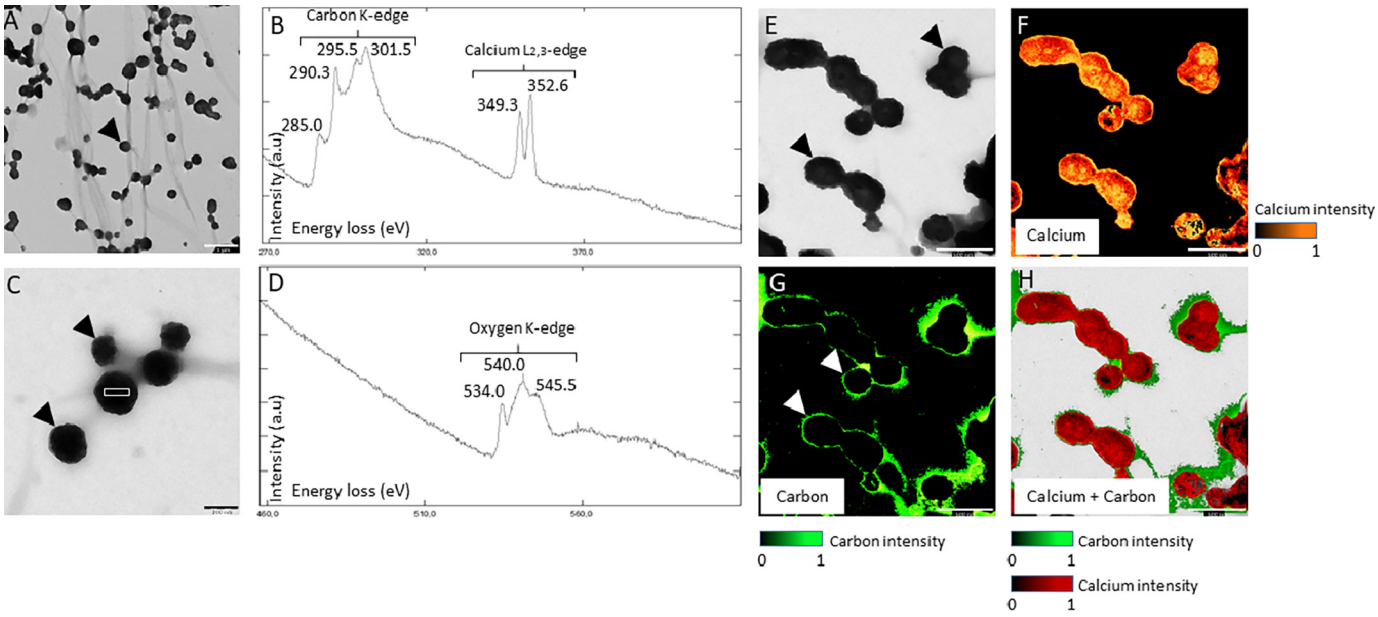

Figure 2. TEM and EELS on UF. *A* and *C,* TEM micrograph of EVs observed in UF. *Black arrowheads* indicate the EVs. *White boxes* indicate EELS analysis area of *B* and *D* graphs. *B* and *D,* EELS spectroscopy on EVs from UF. The carbon K-edge shows three major peaks at 290.3, 295.5, and 301.5 electron volts (eV), characteristic of $CaCO_3$. The peak at 285.0 from the carbon K-edge reflects the presence of organic material. The two peaks 349.3 and 352.6 eV define the calcium L2,3-edge of EELS. The oxygen K-edge displays a major peak at 540.0 specific to the carbonate group (CO_3^{2-}) and two other peaks at 534.0 and 545.5 indicate C = O bond. *E,* TEM micrograph of EV, observed in UF with associated mapping of calcium element (*F*) (324-355 eV). *G,* organic carbon (280-290 eV) and *H,* calcium + carbon combined elements detected by the EELS analysis. *Bars*: *A* = 1 μm, C = 200 nm, *E* to *H* = 500 nm.

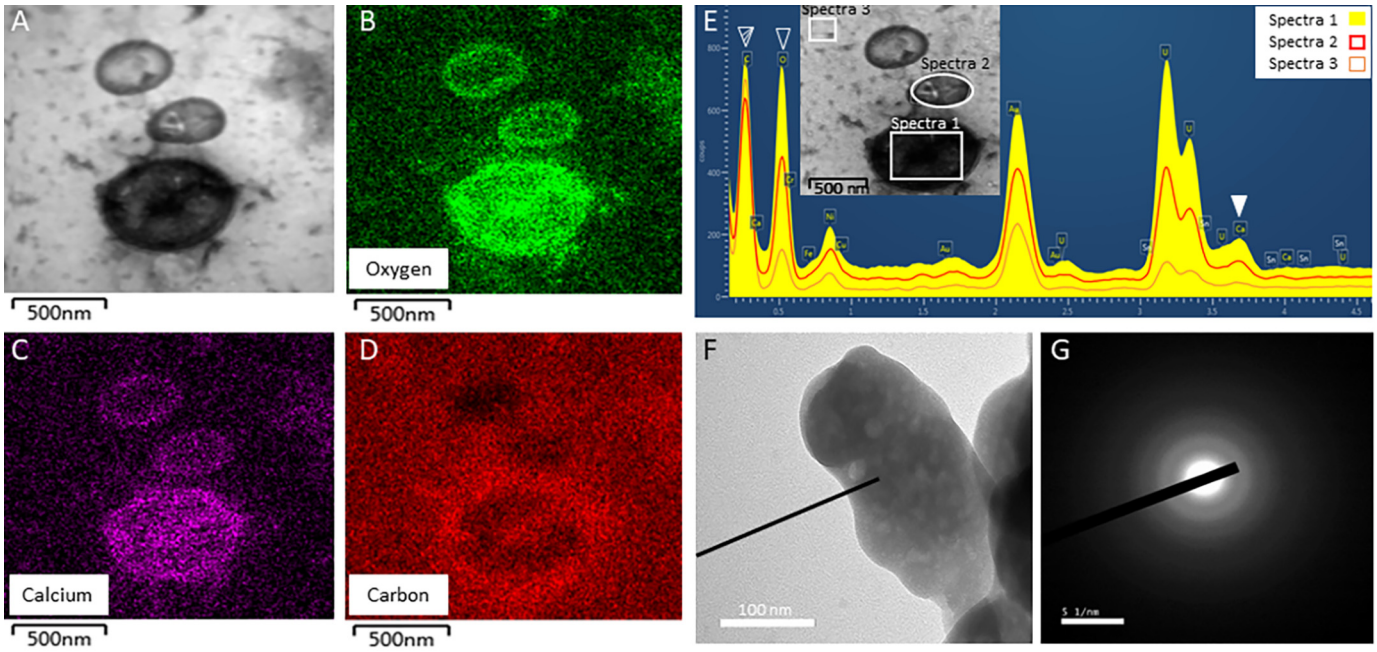

Figure 3. TEM on uterine fluid, EDS and SAED analyses. *A,* TEM of EVs observed in UF fraction at 16 h p.o. with associated mapping of (*B*) oxygen element, (*C*) calcium element, and (*D*) carbon element; as detected by the EDS analysis. *E,* EDS spectrum of the EVs observed in UF and shown in *A*. *Filled white arrowhead* indicates the calcium peak (3.690 keV) of EV, whereas *striped* and *empty white arrowheads* show carbon (0.277 keV) and oxygen (0.525 keV) peaks, respectively. *Boxes* point out the areas of EDS analysis. *F* and *G,* SAED pattern of the mineral detected in EV of UF. Diffuse scattering rings are characteristic of the ACC mineral. *Bars*: *A* to *D* = 500 nm, *F* = 1 μm, *G* = 51 nm.

and proteins) enclose the amorphous calcium carbonate mineral deposits.

The distribution of calcium, carbon, and oxygen in uterine fluid vesicles were also analyzed using EDS (Fig. 3). Oxygen, carbon, and calcium elements co-localized within EVs (Fig. 3, *A–D*). A high C background signal is notable, as samples were mounted on carbon-coated TEM grids. The difference between EDS spectrum 1 (EV), spectrum 2 (EV), and spectrum 3 (background) confirmed the presence of significant amounts of calcium and oxygen inside the EVs, compared with the background signal (Fig. 3*E*).

Indeed, calcium and oxygen signals in the EV were 3- to 5-times higher (spectrum 1) than the background (spectrum 3).

Vesicular mRNA levels in various Gallus gallus tissues

We evaluated the literature on bone and cartilage extracellular vesicles (31–34), EVs (35–38), and the Vesiclepedia database (RRID:SCR_09011), which lists the top 100 proteins that are identified in EVs (39). A total of 33 genes coding for proteins involved in vesicular transport were selected, corresponding to proteins involved as calcium channels to supply calcium, bicarbonate supplier/transporter, chaperone molecules, addressing molecules, intracellular trafficking proteins, extracellular biogenesis and release, and signaling proteins (Table S2). mRNA levels for these 33 genes were quantified in different tissues and organs, namely oviduct segments, bone, duodenum, kidney, and liver (Table 1, Fig. 4). Tissue samples from four specialized oviduct regions were collected to evaluate the mRNA level of EV markers associated with egg white deposition (Ma), eggshell membrane formation (WI), and shell calcification (RI, Ut). Bone was selected as a mineralized tissue (with hydroxyapatite) where EVs have been demonstrated (31, 32, 40, 41). Duodenum (D) and kidney (K) exhibit active ion transport activity without any associated calcification. Finally, liver (L) was selected as an important organ involved in general metabolism. Comparisons of quantified mRNA levels in these organs and tissues were displayed using a heat map diagram (Fig. 4). Z-scores are expressed in terms of mean ± S.D. for each gene. Consequently, the color scale indicates the relative variation of each gene in the different tissues. We observed the highest Z-scores in oviduct segments (Ma, WI, RI, and Ut), for 20 vesicular genes (*Anxa1, Anxa2, Anxa8, Ap1g1, Cd9, Cd82, Edil3, Hspa8, Itgb1, Pdcd6ip, Rab5a, Rab27a, Sdcbp, Tsg101, Vamp3, Vamp7, Vps4, Vps26a, Ywhah,* and *Ywhaz*) compared with the other tissues (Clusters 6 to 8, Fig. 4). *The* mRNA level of genes was also analyzed using ANOVA and Tukey pairwise analysis (Table 1). With the notable exception of *Ap1g1*, all other genes with highest Z-scores in uterus were also significantly different in the same uterine tissue using ANOVA and pairwise analysis (Table 1). Additionally, these statistical tests show that *Itgb1, Sdcbp, Vamp7,* and *Vps4b* were also significantly overexpressed in one or several other tissues (bone (B), kidney (K), and duodenum (D)). *Anxa5, Anxa11, Ap1g1, Hsp90b,* and *Rab7a* were not differentially expressed in the various tissues tested. Both *Rab11a* and *Slc4a7* were significantly over-expressed in D, whereas *Ca2* and *Anxa7* were significantly overexpressed in B and K, respectively, to other tissues. *Arf6* exhibited a significantly higher mRNA level in D and uterus. The remaining three genes *Anxa6*, *Ralb*, and *Vcp* did not exhibit significantly different mRNA levels (Table 1).

Proteomic and Western blotting analyses of EVs

To determine the protein composition of EVs isolated from the UF, we carried out proteomics analysis using nanoLC-MS/MS and verified these observations with Western blotting techniques. Twenty-nine nonredundant proteins were identified in our proteomics analysis (Table 2). Among them, seven proteins correspond to predicted major actors in the hypothetical vesicular transport of ACC (carbonic anhydrase-4 (CA4), EGF-like repeat and discoidin I-like domain-containing protein 3 (EDIL3), ezrin (EZR), programmed cell death 6-interacting protein (PDCD6IP), syntenin-1, ovalbumin (OVA), and lysozyme C (LYZ); Tables 2 and 3) (27). In addition, several Igs and other proteins already identified in chicken eggshell matrix (ovotransferrin, ovalbumin-related X, ovalbumin-related Y, ovocalyxin-25, clusterin, ovomucin, vitelline membrane outer layer protein 1, ovostatin, ovoglobulinG2, prominin-1-A, α2-macroglobulin, and aminopeptidase N) were detected (Table 2). Finally, the angiotensin-converting enzyme precursor (ACE) was also identified.

To confirm EDIL3 proteomic identification, we performed Western blotting analysis on various samples: unfractioned UF (complete), EV fraction of UF (EV fraction), depleted UF (ØEV), and soluble eggshell proteins (SEP) (Fig. 5, *A* and *B*). We also carried out immunoblotting for milk fat globule-EGF factor 8 (MFGE8), because it is another protein potentially involved in guiding EVs during shell mineralization (27). Immunoreactive bands in the vesicle fractions were observed using both antibodies (anti-EDIL3 and anti-MFGE8). Using anti-EDIL3 antibodies, a unique immune band was observed around 60-kDa (54-kDa predicted molecular mass), only in the EV fraction and SEP (Fig. 5*A*). MFGE8 exhibited a single band around 75-kDa (53-kDa predicted molecular mass) in all samples (Fig. 5*B*). The higher than predicted molecular mass observed for both EDIL3 and MFGE8 could be due to post-translational modification, such as glycosylation (27). An MFGE8 immunoband was detected in uterine fluid lacking vesicles, indicating that MFGE8 is soluble in uterine fluid, unlike EDIL3.

Immunofluorescence in uterus for key proteins proposed for UF vesicular transport

Immunofluorescence analysis was performed on chicken uterus sections to localize six proteins (ANXA1, ANXA2, ANXA8, CA4, EDIL3, and PDCD6IP) proposed to play key roles in vesicular transport within the tissue responsible for eggshell mineralization (Fig. 6). Analyses were performed at five defined time points in the eggshell mineralization process. Time points at 5 and 6 h p.o. correspond to the massive accumulation of ACC at the earliest stages of shell formation. At 7 h p.o., ACC is progressively transformed in calcite aggregates, whereas calcite crystals with preferential orientation are fusing at 10 h p.o. to form the compact palisade layer strongly deposited at 16 h p.o. Negative controls demonstrated the absence of nonspecific signals in uterus for all antibodies. EDIL3 and ANXA1 protein levels were maximum at 5 and 6 h p.o., when massive ACC is deposited and then decreased from 7 to 16 h p.o. (Fig. 6). EDIL3 is present in the tubular glands of the lamina propria, whereas ANXA1 was localized to the epithelium. A faint immunostaining was obtained for ANXA2 at 5 h p.o., whereas the signal was stronger at 6, 7, and 10 h p.o. in the epithelium (Fig. 6), then decreased at 16 h p.o. ANXA8 was

Table 1

Normalized vesicular mRNA levels in the four oviduct regions and other tissues

Messenger RNA level results are reported as mean ± S.D. Messenger RNA level was assessed during the active growth phase of eggshell mineralization at 10 h p.o. except for B at 18 h p.o. Following reverse transcription, the mRNA level was quantified using primers designed with Primer-blast tool of NCBI (RRID:SCR_003095) and validated for the Biomark microfluidic system (BMK-M-96.96; Fluidigm). Relative quantification was normalized with eight housekeeping genes using GenNorm software. Superscript letters "a" to "e" correspond to significance results of the ANOVA-Tukey tests with "a" the letter corresponding to the highest level of mRNA for each gene. Tibial bone, *B*; duodenum, *D*; kidney, *K*; liver, *L*; magnum, *Ma*; white isthmus, *WI*; red isthmus, *RI*; uterus, *Ut*. The gene accession numbers and primer sequences are compiled in Table S3.

		Tissues				Oviduct segments				
Function	Gene	B	D	K	L	Ma	WI	RI	Ut	ANOVA *p* value
Calcium channel	*Anxa1*	0.205 ± 0.200^{cd}	0.002 ± 0.001^{d}	0.009 ± 0.004^{d}	0.001 ± 0.001^{d}	0.194 ± 0.066^{cd}	2.190 ± 0.749^{b}	3.338 ± 0.768^{a}	0.891 ± 0.320^{c}	<0.001
	Anxa2	0.307 ± 0.240^{cd}	0.521 ± 0.180^{cd}	0.006 ± 0.009^{d}	0.001 ± 0.002^{d}	0.543 ± 0.340^{cd}	1.208 ± 0.805^{bc}	2.884 ± 1.247^{a}	1.904 ± 0.459^{ab}	<0.001
	Anxa5	0.431 ± 0.359	0.401 ± 0.289	0.189 ± 0.173	1.462 ± 0.828	2.001 ± 2.920	0.560 ± 0.298	1.405 ± 1.044	0.298 ± 0.193	0.068
	Anxa6	2.116 ± 1.522^{ab}	0.446 ± 0.282^{b}	0.313 ± 0.163^{b}	1.473 ± 0.558^{ab}	1.328 ± 1.140^{ab}	0.478 ± 0.375^{ab}	0.347 ± 0.147^{b}	0.543 ± 0.437^{ab}	0.008
	Anxa7	0.206 ± 0.081^{cd}	1.436 ± 0.306^{b}	7.074 ± 1.170^{a}	0.191 ± 0.059^{d}	0.623 ± 0.330^{bcd}	0.676 ± 0.410^{bcd}	1.122 ± 0.284^{bc}	1.450 ± 0.526^{b}	<0.001
	Anxa8	0.026 ± 0.029^{d}	0.001 ± 0.001^{d}	0.001 ± 0.001^{d}	0.001 ± 0.001^{d}	1.669 ± 0.922^{bc}	2.513 ± 1.205^{ab}	3.958 ± 1.720^{a}	0.979 ± 0.344^{cd}	<0.001
	Anxa11	0.214 ± 0.044	0.562 ± 0.152	0.644 ± 0.293	0.916 ± 0.939	3.760 ± 6.150	2.180 ± 3.080	1.615 ± 1.436	1.008 ± 0.647	0.236
Bicarbonate supplier/transporter	Ca^{2+}	21.440 ± 10.270^{a}	2.585 ± 1.127^{b}	1.633 ± 0.834^{b}	0.512 ± 0.157^{b}	0.763 ± 0.196^{b}	1.149 ± 0.297^{b}	0.561 ± 0.171^{b}	1.131 ± 0.394^{b}	<0.001
	Slc4a7	0.115 ± 0.039^{cd}	1.905 ± 0.665^{a}	0.069 ± 0.008^{cd}	0.012 ± 0.007^{d}	0.454 ± 0.149^{cd}	0.551 ± 0.287^{c}	1.078 ± 0.262^{b}	0.529 ± 0.120^{c}	<0.001
Membrane organizer	*Cd82*	0.634 ± 0.345^{cd}	0.769 ± 0.310^{bcd}	0.367 ± 0.241^{cd}	0.162 ± 0.141^{d}	1.598 ± 0.970^{ab}	0.943 ± 0.260^{abcd}	1.270 ± 0.403^{abc}	1.865 ± 0.834^{a}	<0.001
	Cd9	0.085 ± 0.100^{b}	0.258 ± 0.129^{b}	0.403 ± 0.168^{b}	0.053 ± 0.068^{b}	1.751 ± 1.255^{b}	12.900 ± 4.98^{a}	1.780 ± 0.323^{b}	1.617 ± 1.106^{b}	<0.001
Chaperone	*Hsp90b1*	2.427 ± 1.776^{a}	0.941 ± 0.672^{a}	3.230 ± 3.500^{a}	5.250 ± 3.920^{a}	4.560 ± 4.650^{a}	1.649 ± 0.760^{a}	1.627 ± 0.659^{a}	2.992 ± 0.840^{a}	0.039
	Hspa8	0.562 ± 0.125^{d}	0.840 ± 0.203^{bcd}	1.180 ± 0.334^{b}	0.404 ± 0.151^{d}	0.973 ± 0.249^{bc}	0.919 ± 0.287^{bc}	1.709 ± 0.399^{a}	1.084 ± 0.205^{b}	<0.001
Adhesion molecule	*Itgb1*	1.925 ± 0.947^{a}	0.345 ± 0.084^{bc}	0.671 ± 0.491^{abc}	0.133 ± 0.064^{c}	1.827 ± 0.961^{a}	1.536 ± 0.826^{ab}	1.783 ± 1.054^{a}	1.396 ± 0.504^{abc}	<0.001
	Edil3	0.019 ± 0.017^{b}	0.000 ± 0.000^{b}	0.001 ± 0.003^{b}	0.000 ± 0.000^{b}	0.000 ± 0.000^{b}	0.825 ± 0.303^{a}	1.101 ± 0.737^{a}	0.737 ± 0.464^{a}	<0.001
	Mfg8	0.514 ± 0.380^{c}	0.114 ± 0.078^{c}	0.856 ± 0.208^{c}	4.373 ± 1.223^{a}	0.029 ± 0.063^{c}	0.803 ± 0.399^{c}	2.139 ± 1.194^{b}	0.381 ± 0.385^{c}	<0.001
Intracellular trafficking	*Rab11a*	0.399 ± 0.125^{d}	2.575 ± 0.600^{a}	0.993 ± 0.110^{b}	0.506 ± 0.079^{cd}	1.110 ± 0.201^{b}	0.703 ± 0.130^{bcd}	0.952 ± 0.076^{bc}	1.116 ± 0.226^{b}	<0.001
	Rab27a	0.381 ± 0.168^{c}	0.329 ± 0.197^{c}	0.585 ± 0.283^{c}	0.185 ± 0.144^{c}	2.306 ± 1.363^{a}	1.778 ± 0.517^{ab}	1.090 ± 0.485^{bc}	1.742 ± 0.634^{ab}	<0.001
	Rab5a	0.525 ± 0.353^{bc}	0.779 ± 0.251^{bc}	0.784 ± 0.324^{bc}	0.780 ± 0.422^{bc}	1.701 ± 0.881^{a}	1.337 ± 0.500^{abc}	1.294 ± 0.300^{abc}	1.649 ± 0.596^{ab}	<0.001
	Rab7a	1.879 ± 0.849	1.399 ± 0.781	0.991 ± 0.381	1.016 ± 0.500	1.375 ± 0.523	1.258 ± 0.335	1.353 ± 0.377	1.509 ± 0.354	0.297
	Ralb	0.987 ± 0.257^{ab}	1.034 ± 0.658^{ab}	1.350 ± 0.587^{a}	1.191 ± 0.484^{ab}	0.679 ± 0.939^{ab}	0.615 ± 0.371^{ab}	0.644 ± 0.438^{ab}	0.349 ± 0.203^{b}	0.039
	Vcp	1.116 ± 0.495^{ab}	0.414 ± 0.136^{b}	0.707 ± 0.259^{b}	2.129 ± 0.802^{a}	1.379 ± 1.746^{ab}	1.071 ± 0.350^{ab}	1.229 ± 0.469^{ab}	1.334 ± 0.519^{ab}	0.027
	Arf6	0.597 ± 0.141^{bc}	1.688 ± 0.490^{a}	0.770 ± 0.201^{bc}	0.702 ± 0.360^{bc}	0.647 ± 0.255^{bc}	0.453 ± 0.194^{c}	0.949 ± 0.305^{bc}	1.206 ± 0.370^{ab}	<0.001
	Sdcbp	0.581 ± 0.203^{d}	0.920 ± 0.225^{cd}	2.398 ± 0.326^{ab}	0.546 ± 0.210^{d}	2.585 ± 1.130^{a}	2.506 ± 0.629^{ab}	2.013 ± 0.386^{ab}	1.567 ± 0.422^{bc}	<0.001
EV biogenesis	*Tsg101*	0.134 ± 0.018^{e}	0.510 ± 0.136^{cd}	0.764 ± 0.180^{bc}	0.386 ± 0.056^{de}	1.206 ± 0.385^{a}	0.900 ± 0.224^{ab}	1.088 ± 0.134^{ab}	1.192 ± 0.184^{a}	<0.001
	Vps26a	0.447 ± 0.271^{de}	0.831 ± 0.186^{cde}	1.078 ± 0.147^{bcd}	0.466 ± 0.183^{de}	1.203 ± 0.419^{abcd}	1.754 ± 0.338^{ab}	1.937 ± 0.657^{a}	1.417 ± 0.771^{abc}	<0.001
	Pdcd6ip	0.213 ± 0.047^{e}	1.150 ± 0.225^{bc}	0.727 ± 0.156^{cde}	0.493 ± 0.109^{de}	0.777 ± 0.332^{cd}	0.842 ± 0.303^{cd}	1.454 ± 0.301^{b}	2.030 ± 0.545^{a}	<0.001
EV release	*Vamp3*	0.199 ± 0.060^{d}	0.575 ± 0.088^{bc}	0.365 ± 0.124^{cd}	0.156 ± 0.080^{d}	0.682 ± 0.190^{b}	0.751 ± 0.122^{b}	1.117 ± 0.253^{a}	0.749 ± 0.134^{b}	<0.001
	Vamp7	0.439 ± 0.224^{de}	0.590 ± 0.281^{cde}	1.527 ± 0.542^{ab}	1.088 ± 0.258^{abcd}	0.911 ± 0.258^{bcde}	1.198 ± 0.242^{abc}	1.407 ± 0.552^{ab}	1.704 ± 0.373^{a}	<0.001
	Vps4b	0.014 ± 0.010^{b}	0.041 ± 0.020^{ab}	0.019 ± 0.019^{b}	0.009 ± 0.006^{b}	0.052 ± 0.029^{ab}	0.028 ± 0.022^{b}	0.029 ± 0.017^{b}	0.090 ± 0.069^{a}	<0.001
	Ap1g1	0.613 ± 0.163^{ab}	0.649 ± 0.154^{ab}	0.509 ± 0.097^{ab}	0.334 ± 0.185^{b}	0.824 ± 0.539^{ab}	0.726 ± 0.404^{ab}	1.063 ± 0.260^{ab}	1.199 ± 0.465^{ab}	0.030
Signaling protein	*Ywhah*	0.338 ± 0.089^{abcd}	0.517 ± 0.310^{abcd}	0.171 ± 0.104^{cd}	0.111 ± 0.098^{d}	0.970 ± 0.339^{ab}	1.071 ± 0.683^{ab}	1.089 ± 0.562^{a}	0.872 ± 0.568^{abc}	<0.001
	Ywhaz	0.485 ± 0.200^{cd}	0.501 ± 0.152^{cd}	0.507 ± 0.131^{cd}	0.136 ± 0.050^{d}	0.660 ± 0.266^{c}	0.786 ± 0.159^{bc}	1.192 ± 0.291^{b}	2.121 ± 0.394^{a}	<0.001

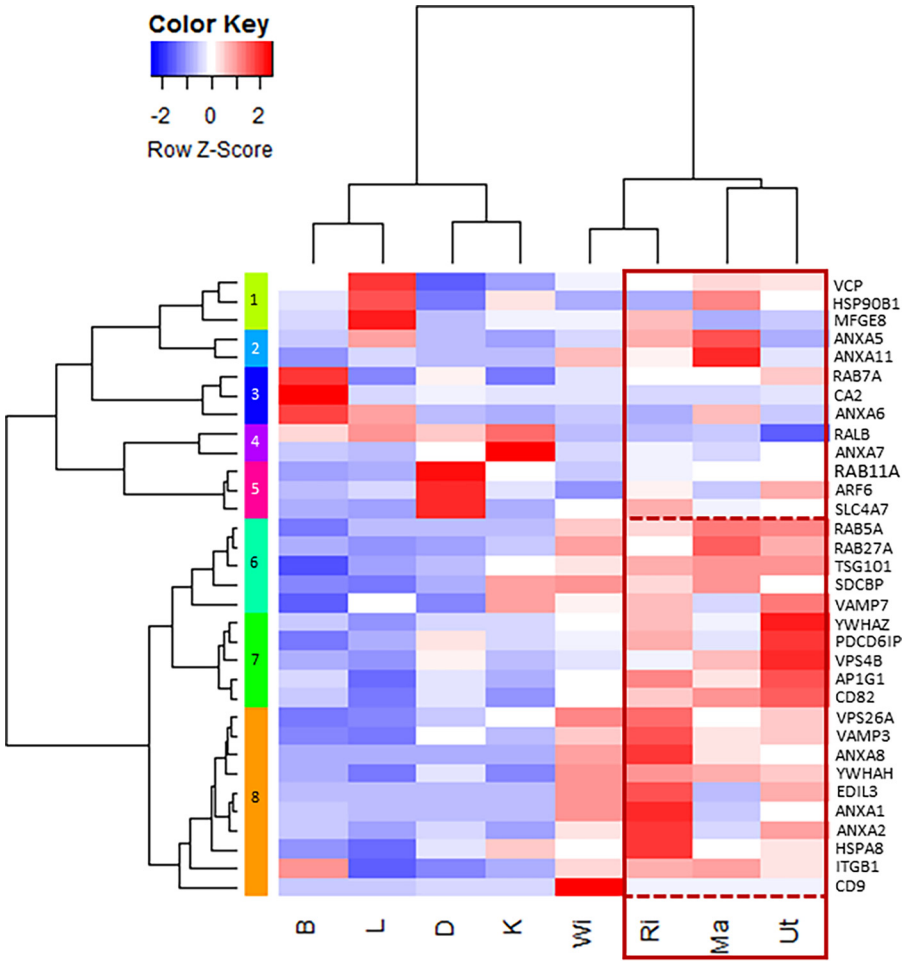

Figure 4. Heat map of vesicular mRNA levels in the four oviduct segments (Ma, WI, RI, and Ut) and four tissues (*B*, bone; *D*, duodenum; *K*, kidney; *L*, liver). Z-score range was colored from *blue* (*−2 Row*, Z-Score, low mRNA level) to *white* (*0 Row*, Z-Score, intermediate mRNA level) and to *red* (*2 Row*, Z-score, high mRNA level). Gene accessions and primers are reported in Table S3.

detected in both tubular glands and epithelium regions at each stage of mineralization, with a maximum signal at 10 h p.o. (Fig. 6). A strong CA4 signal was observed in the epithelial cells at 5 h, at 6 h when massive accumulation of ACC occurred, and at 7 h p.o. when a dissolution process allowed ACC transformation in calcite, whereas the signal was low at 16 h p.o. PDCD6IP immunofluorescence revealed that the protein was largely localized in the epithelium throughout the biomineralization process (5 to 16 h p.o.) (Fig. 6).

Discussion

Vesicles in hen oviduct

EVs are defined as phospholipid-enclosed nanoparticles (30–2000 nm) that carry a complex and variable cargo of biological contents including proteins and nucleic acids (36). EVs have been categorized as exosomes (30-150 nm) released by exocytosis, apoptotic bodies (50-5000 nm) released at the later stages of cell apoptosis, and shedding microvesicles or ectosomes (100-1000 nm) secreted by outward budding of the plasma membrane (42). Diverse biological functions have been ascribed to EVs, which vary according to the parental cell from which they were derived and the local microenvironment (36). Indeed, EVs have been implicated in numerous processes, such as tissue formation, as well as in pathological conditions, including vascular calcification and many forms of cancer (36). They have been isolated from many biological fluids and recent reviews highlight their biological significance for intercellular communication and during pathological (43–48).

Recently, EVs have been reported to play potential roles in preserving sperm function within the hen genital tract and mediate interaction with sperm (49). Avian species have sperm reservoirs called sperm storage tubules (SST), which are mainly located in the mucosa of the utero-vaginal junction. Exosomes were observed both at the surface epithelium and inside SST using EM. Moreover, exosomes have been isolated from the avian uterine fluid and then observed using EM (49).

The role of vesicles in the transport of mineralizing ions during biomineralization has been reported in both invertebrate and vertebrate systems. The most documented vesicular mediated mineralization systems are in vertebrate skeleton and teeth, for which vesicles associated with calcium phosphate have been described (40, 41, 50). However, vesicular-mediated calcium carbonate mineralization has only been reported in invertebrates. Sea urchin spicules are the best documented example of invertebrate calcite biomineralization mediated by

Table 2

List of the 29 proteins identified by nanoLC-MS/MS analysis in uterine fluid EVs

The EV fraction was purified from uterine fluid (UF) collected at 9 h p.o.

No.	Identified proteins	Symbols	GenBank accession number	Gene ID	Theoretical molecular mass	Normalized weighted spectra	emPAI
1	Cluster of ovalbumin	OVA	AUD54558.1	396058	43 kDa	1 031.10	29.909
2	Cluster of ovotransferrin	OVOT	P02789.2	396241	78 kDa	560	8.219
3	Cluster of ovomucin	MUC	NP_989992.1	395381	234 kDa	448.91	0.82205
4	Cluster of α2-macroglobulin-like	A2M	XP_025007673.1	418254	158 kDa	288	0.89983
5	Cluster of ovomacroglobulin (ovostatin)	OVST	CAA55385.1	396151	164 kDa	215	0.47326
6	Ig μ chain C region	NA[a]	P01875.2	NA	48 kDa	210	2.499
7	Immunoglobulin α heavy chain	NA	AAB22614.2	NA	62 kDa	70	0.96212
8	Ig light chain	NA	AAA48859.1	416928	25 kDa	63	0.88882
9	Ovalbumin-related Y	OVAL-Y	BAM13279.1	420897	44 kDa	66	0.66086
10	Polymeric immunoglobulin receptor	PIGR	AAQ14493.1	419848	71 kDa	71	0.31136
11	Ovoglobulin G2	OVOG2/TENP	BAM13270.1	395882	47 kDa	66	0.59817
12	Cluster of immunoglobulin light chain variable region	NA	AJQ23663.1	NA	11 kDa	42	0.87697
13	Cluster of anti-prostate specific antigen antibody immunoglobulin variable region	NA	AL× 37966.1	NA	13 kDa	51	1.4661
14	Cluster of programmed cell death 6-interacting protein	PDCD6IP	XP_015137020.1	420725	97 kDa	46	0.16725
15	Cluster of immunoglobulin light chain variable region	N/A	AJQ23661.1	NA	11 kDa	34	1.2195
16	Cluster of lysozyme C	LYZ	P00698.1	396218	16 kDa	41	1.2327
17	Clusterin	CLU	NP_990231.1	395722	51 kDa	7	0.36338
18	Cluster of ovalbumin-related protein X	OVAL-X	NP_001263315.1	420898	44 kDa	16	0.35247
19	Carbonic anhydrase 4	CA4	XP_415893.1	417647	36 kDa	23	0.5467
20	Cluster of ezrin	EZR	NP_990216.1	395701	69 kDa	13	0.20218
21	Uncharacterized protein LOC771972 (OC× 25)	OCX25	XP_001235178.3	771972	27 kDa	10	0.41449
22	EGF-like repeat and discoidin I-like domain-containing protein 3	EDIL3	XP_424906.3	427326	54 kDa	12	0.2673
23	Immunoglobulin heavy chain V-region	NA	AAA48830.1	NA	11 kDa	9	1.2444
24	Cluster of syntenin-1	SDCBP	NP_001026195.1	421136	32 kDa	11	0.21673
25	Aminopeptidase N	AMPN	ACZ95799.1	395667	109 kDa	6	0.060894
26	Cluster of immunoglobulin light chain variable region	NA	AJQ23760.1	NA	10 kDa	6	0.75959
27	Prominin-1-A	PROM1	XP_004942263.1	423849	88 kDa	3	0.075475
28	Angiotensin-converting enzyme precursor	ACE	NP_001161204.1	419953	147 kDa	5	0.044662
29	Vitelline membrane outer layer protein 1	VMO1	NP_001161233.1	418974	20 kDa	4	0.35873

[a]NA, not applicable.

Table 3

Proteins of the proposed ACC extracellular vesicle system detected by nanoLC-MS/MS analysis

Scaffold software in uterine fluid EVs. The EV fraction was purified from uterine fluid (UF) collected at 9 h p.o. The entire set of detected proteins is listed in Table 2 Indicated accessions correspond to the GenBank accession number. HCO_3^-, bicarbonate ion. Vesiclepedia database (RRID:SCR_019011) classifies the proteins that are frequently identified in EVs. EV localization was predicted using molecular function of proteins on Uniprot (RRID:SCR_002380). References used were 31–34, 70–73, 75, and 77–86.

Protein Name	GenBank accession number	Gene ID	Molecular mass	Proposed role in UF EVs	EV localization	Vesiclepedia rank	Bone/cartilage EV references	Eggshell/UF proteome references
CA4	XP_415893.1	417647	36 kDa	HCO_3^- supplier	Membrane: glycosylphosphatidylinositol (glycosylphosphatidylinositol-anchored)	NA[a]	NA	62, 67, 74, 76, 78
EDIL3	XP_424906.3	427326	54 kDa	Targeting protein	Membrane: phosphatidylserine-binding	NA	34	63, 65, 67, 70, 71, 72, 73, 75, 76, 78
Ezrin	NP_990216.1	395701	69 kDa	Membrane fusion (plasma membrane-cytoskeleton linker)	Membrane: phosphatidylinositol 4,5 bisphosphate-binding	30/100	33, 34, 35	62, 63, 74, 78
PDCD6IP	XP_015137020.1	420725	97 kDa	EV biogenesis	Lumen: incorporation	1/100	32, 33	62, 77, 78
Syntenin-1	NP_001026195.1	421136	32 kDa	EV biogenesis	Membrane: phosphatidylinositol 4,5 bisphosphate-binding	19/100	32, 33, 34	62, 63, 64, 74, 75, 78
Ovalbumin	AUD54558.1	NA	43 kDa	ACC stabilization	Lumen: incorporation	NA	NA	62, 63, 65, 67, 69, 70, 74, 75, 76
Lysozyme C	P00698.1	396218	16 kDa	ACC stabilization	Lumen: incorporation	NA	34	62, 63, 65, 67, 69, 70, 74, 75, 76, 78

[a]NA, not applicable.

vesicles (6, 51). The involvement of vesicles was also proposed but not confirmed for molluscan shell formation (7) and coral exoskeletons (8).

Eggshell mineralization and vesicular transport

Five to six g of calcium carbonate was deposited within an 18-h period during chicken egg formation. This requires rapid delivery of large amounts of calcium and carbonate, representing 10% (2 g) of hen total body calcium exported each day (24). Neither component (Ca^{2+} or HCO_3^-) is stored in the uterus, but rather are continuously supplied during eggshell formation from the blood plasma via transport across the uterine glandular cells. Mechanisms of transepithelial transfer of calcium and bicarbonates have been widely studied and represent the current accepted model for eggshell mineralization (21, 24, 25). Recently, intestinal paracellular transfer of calcium during

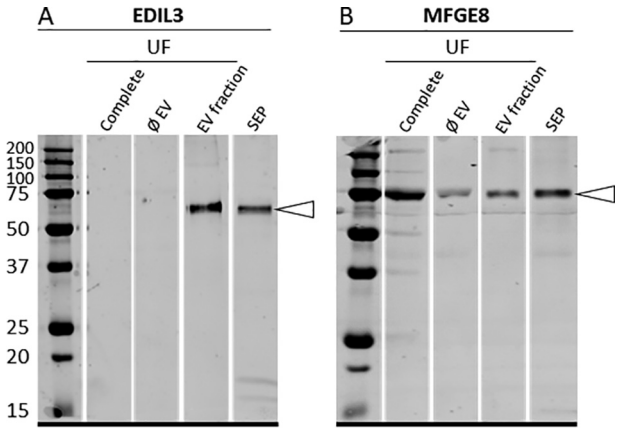

Figure 5. Western blotting analysis of (*A*) EDIL3 and (*B*) MFGE8 in UF: unfractioned UF (*complete*), depleted UF (*ØEV*), EV fraction of UF (*EV fraction*), and SEP. Proteins (15 μg) were subjected to 12.5% SDS-PAGE electrophoresis and blotted for analysis. The membranes were probed with (*A*) rabbit polyclonal anti-EDIL3 (1:1,000, SAB2105802, Sigma-Aldrich, Saint-Quentin Fallavier, France) and (*B*) rabbit synthetic anti-MFGE8 peptide (1:1,000, rabbit polyclonal; ProteoGenix, Schiltigheim). *White arrowheads* indicate the immunoreactive bands.

eggshell formation was demonstrated (52), raising the possibility of paracellular transfer of calcium in uterus as well; however, no experimental data addressing this possibility is yet available. The vesicular transport of calcium as stabilized ACC is a third complementary pathway to transfer calcium and carbonate to the calcification site.

Shell calcification, which takes place in a saturated milieu (uterine fluid) (53), is initiated with the accumulation of ACC deposits on the eggshell membranes during 5–7 h p.o. (26). We have recently proposed a novel model for avian eggshell biomineralization involving EVs budding from uterine epithelial cells, which transit through the UF and deliver stabilized ACC mineral to the eggshell membranes and mineralization front (29). One attractive advantage of this mechanism is that non-specific precipitation in the fluid cannot occur. In this study, we report additional experimental support for this model. We demonstrate the presence of EVs containing ACC in UF, and we define some of the molecular actors involved in this process (Fig. 7). Moreover, we observed vesicles from 100 to 500 nm in the uterine cell cytoplasm and their accumulation at the apical membranes. We also observed budding from uterine cells to secrete these vesicles into uterine fluid. The size of vesicles observed in both fluid and uterine cells, and their outward budding, confirmed that EVs similar to shedding microvesicles or ectosomes are present. Secretory activity of multivesicular bodies has been described at the hen utero-vaginal junction, where spermatozoa are preserved in specialized glands (54). Therefore, the distinct oviduct segments seem to use vesicles for different functions (*i.e.* sperm preservation and secretion of mineral precursors). Moreover, it is intriguing that 250-300–nm granules have been detected within the calcium reserve body sac of the mineralized mammillary cones (55), which could correspond to trapped mineralization-specific EVs.

This study also gives new important insight on the stabilization and delivery of ACC to the mineralization site where the final structure of eggshell is completed. The avian eggshell is a highly ordered structure, consisting of a porous bioceramic resulting from the sequential deposition of calcium carbonate and organic matrix in the red isthmus/uterus regions of the distal oviduct (15, 17, 23, 56–58). Eggshell mineralization results from the aggregation of ACC particles and their transformation into calcite crystals to allow a very rapid and controlled process. Additionally, ACC, which is highly unstable under physiological conditions, must be stabilized in this milieu. In the present study, both EELS and EDS spectroscopy confirmed the presence of calcium carbonate mineral deposits within the vesicles. Furthermore, selected area electron diffraction confirmed the amorphous nature of calcium carbonate. Intracellular vesicles containing ACC were previously observed inside sea urchin epithelial cells (6, 59, 60). In vertebrates, amorphous calcium phosphate has been observed *in vivo* inside intracellular vesicles in embryonic mouse osteoblasts (61). Extracellular vesicles with mineral were also reported for embryonic chick femur (62) and growth plate cartilage of chicken (63, 64). As an extension of these observations, we suggest that ACC is packaged inside vesicles when they are formed within the uterine cells. In other biomineralization models, it is known that intracellular calcium is stored in the endoplasmic reticulum (65). However, the subcellular source of ACC-containing EVs detected in our study remains unclear.

Expression of vesicular transport actors

The experimental evidence from this study is summarized in a diagram of ACC vesicular transport to the mineralizing site, in which the main identified vesicular actors are incorporated (Fig. 7). Among the genes that we investigated, annexins can function as calcium channels (66–69), to enable uptake of the calcium ions required for intravesicular ACC formation. Three of them (*Anxa1, -2* and *-8*) were highly expressed in the oviduct segments where eggshell calcification takes place (Ut and RI) (Fig. 8), and were overabundant at the initial phase of shell mineralization (5–10 h p.o.), compared with later stages. ANXA1 (21, 70), ANXA2 (21, 25, 71–73), and ANXA8 (70, 73) have been reported in chicken eggshell proteomic and transcriptomic surveys (70). ANXA1, ANXA2, and ANXA8 could bind to EV membranes via their phospholipid-binding domain (74). These three annexins constitute, therefore, excellent candidates as participants in vesicular transport, where they could mediate the entry and accumulation of calcium.

Bicarbonate is a precursor for the calcium carbonate of avian eggshells, and consequently we investigated carbonic anhydrase 2 and 4 (CA2 and CA4) and sodium bicarbonate cotransporter 3 (SLC4A7), as bicarbonate suppliers in vesicular transport, because these have previously detected in uterine transcriptomes during eggshell calcification (21, 25). In our study, *Ca2* was not significantly overexpressed in tissues where the shell is mineralized (RI and Ut); however, we noted that CA4 was previously identified in chicken eggshell proteomes (70, 71, 75). We observed that *Ca4* was expressed in duodenum, kidney, and magnum, in addition to Ut where eggshell calcification occurs (Fig. 8). The presence of CA4 protein in the uterine epithelial cells was confirmed by immunofluorescence, and was overabundant at the onset of shell calcification compared with later stages. Finally, proteomic analysis of purified UF EVs

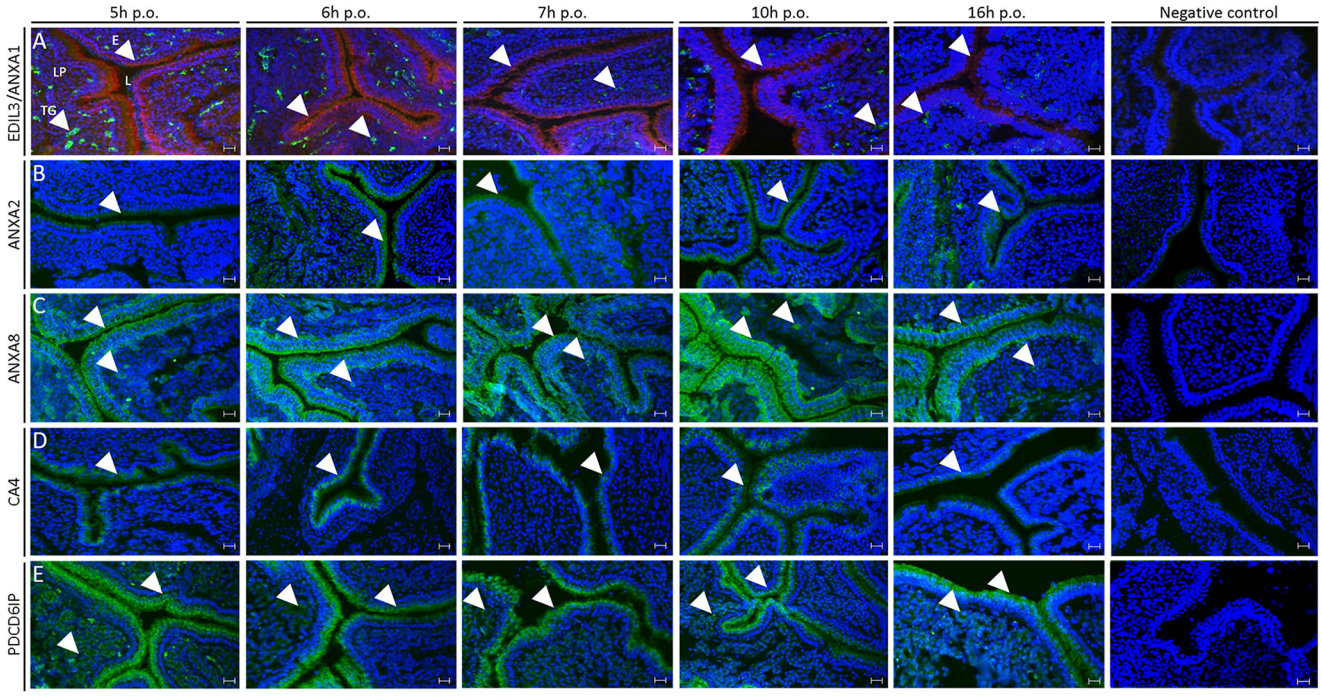

Figure 6. Immunofluorescence of ANXA1, ANXA2, ANXA8, EDIL3, CA4, and PDCD6IP in chicken uterus. The respective rows correspond to: *A,* co-staining of ANXA1 (*red*) and EDIL3 (*green*), *B,* staining of ANXA2 (*green*); *C,* staining of ANXA8 (*green*); *D,* staining of CA4 (*green*); and *E,* staining of PDCD6IP (*green*). ANXA1, ANXA2, and CA4 were localized in the epithelium. ANXA8 and PDCD6IP signals were observed in both epithelium and tubular glands of lamina propria. EDIL3 was solely detected in tubular glands. *E,* ciliated and glandular epithelium; *L,* lumen; *LP*, lamina propria; *TG*, tubular glands. The primary and secondary antibodies are compiled in Table S4. *Bars*, 100 μm. *White arrowheads* indicate positive signal in either tubular glands or epithelium.

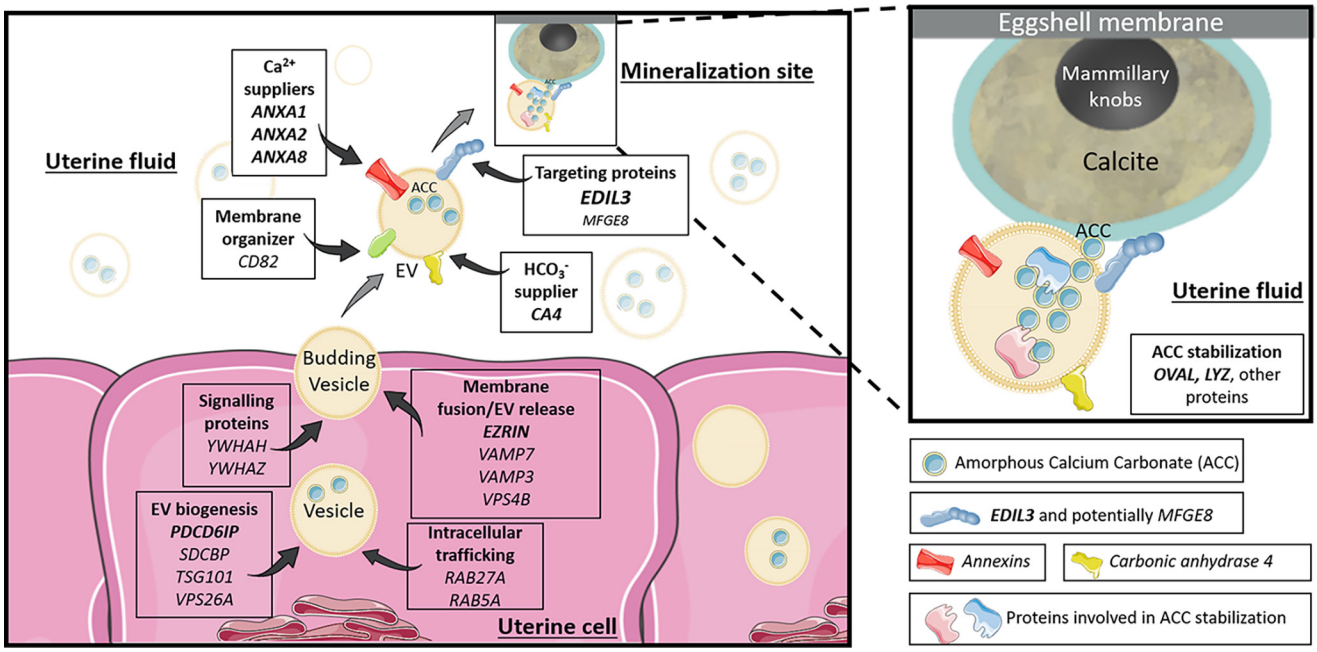

Figure 7. Proposed vesicular function for the different genes and proteins investigated in the study. The EVs bud by exocytosis from the plasma membrane of the uterine cells. ANXA1, -2, -8, and CA4 supply calcium and bicarbonate ions, respectively (inside uterine cells or in the UF). The EVs transit the UF to deliver stabilized ACC to the mineralization sites. The passage of EV-encapsulated ACC avoids nonspecific precipitation in the UF and provides stabilized ACC to the mineralization sites. OVA and LYZ stabilize ACC inside vesicles. EDIL3 (in *bold*), and to a lesser extent MFGE8, guide the EVs by targeting calcium to the mineralization front. The rest of the proteins are involved in EV biology (biogenesis, intracellular transport, and release). The genes in *bold* represent proteins identified in our proteomic and/or immunofluorescence analyses. Elements were from Servier Medical Art (https://smart.servier.com/), licensed under a Creative Commons Attribution 3.0 Unported License.

confirmed that CA4 is present in vesicles. CA4 is a glycosylphosphatidylinositol-linked protein (76), and could be anchored to the outside of vesicle membranes and catalyze the reversible hydration of CO_2 into HCO_3^- at this location. We propose that the CA4-catalyzed accumulation of high levels of bicarbonate in proximity to the vesicular stores of Ca would

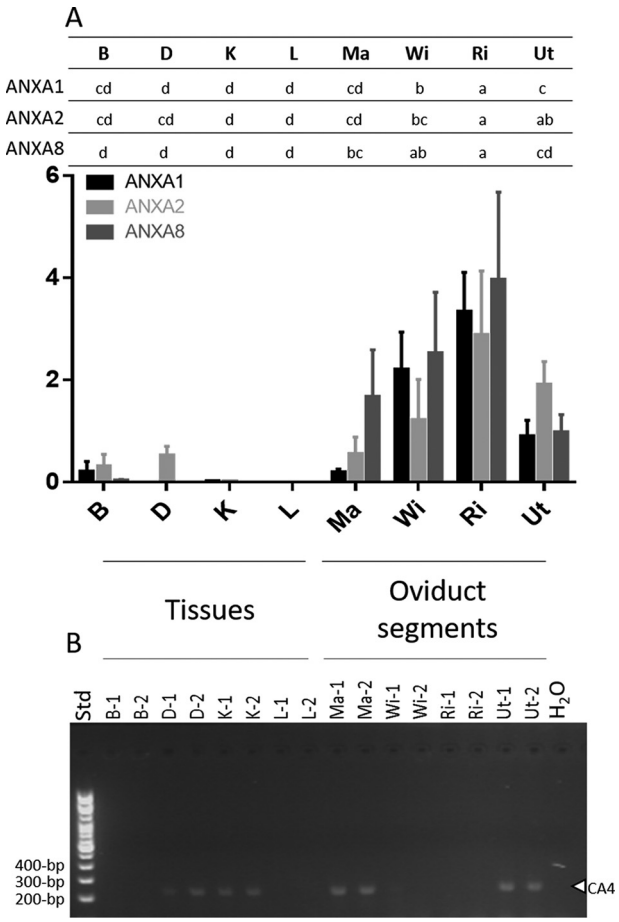

Figure 8. mRNA levels of annexins (*ANX*) and CA4. *A, Anxa1, Anxa2,* and *Anxa8* mRNA levels. Following reverse transcription, mRNA level was quantified using the Biomark microfluidic system (BMK-M-96.96; Fluidigm); $n = 6$. Relative quantification was normalized with eight housekeeping genes using GenNorm software. *B, Ca4* RT-PCR (100-bp DNA ladder). mRNA level was assessed during the active growth phase of mineralization 10 h p.o. except for *B* at 18 h p.o. Tibial bone, *B*; duodenum, *D*; kidney, *K*; liver, *L*; magnum, *Ma*; white isthmus, *Wi*; red isthmus; *Ri*; uterus, *Ut*; H_2O, negative control; *Std*, size (bp) of DNA ladder (100-bp); $n = 2$. *Letters at the top* indicate statistically significant differences in ANXs mRNA levels between the tissues (ANOVA-Tukey). The gene accession numbers and primers are compiled in Table S3. GraphPad Prism software was used for diagram representation.

promote the formation of intravesicular ACC. SLC4A7 is a sodium bicarbonate cotransporter containing transmembrane domains (RRID:SCR_002380), which was identified in matrix vesicles released from mineralizing human osteoblast-like cells (34). Although SLC4A7 expression was detected in chicken uterus by RNA-Seq (https://anr.fr/Projet-ANR-13-BSV6-0007), in this study we observed that it was not significantly overexpressed in RI and Ut.

We also quantified the mRNA levels of numerous additional vesicle markers within uterine epithelial cells. Among the 20 vesicular genes highly expressed in RI and Ut, seven encode proteins ranked in the top 100 of EV protein markers by Vesiclepedia (Table S2). These seven proteins encoded by *Pdcd6ip, Hspa8, Anxa2, Ywhaz, Sdcbp, Tsg101*, and *Anxa1* are, respectively, reported to rank 1st, 3rd, 5th, 13th, 19th, 39th, and 43th by Vesiclepedia (39), and were previously reported as constituents of the avian eggshell proteome (Table S2) (70–73, 77–86). Moreover, 12 vesicular genes (*Anxa1, Anxa2, Cd82, Edil3, Hspa8, Pdcd6ip, Rab5a, Sdcbp, Tsg101, Vamp7, Ywhah*, and *Ywhaz*) encode proteins previously detected in exosomes or matrix vesicles of bone cells, mineralizing cartilage or articular cartilage (Table S2) (31–34, 87). The 20 genes that are highly expressed in oviduct segments responsible for eggshell mineralization encode proteins that have been incorporated into our eggshell vesicular transport model (Fig. 7, Table S2). Some are involved in the general functioning of EVs such as vesicle formation and/or trafficking. Indeed, the genes *Pdcd6ip, Sdcbp, Tsg101,* and *Vps26a* encode proteins involved in the biogenesis of EVs (32, 35–38). Proteins encoded by *Rab5a, Rab27a, Vamp7, Vamp3,* and *Vps4b* participate in membrane fusion/vesicle release (32, 35, 36, 38). *Yhwah* and *Ywhaz* encode signaling proteins (32), whereas *Hspa8* and *Cd82* encode chaperone and membrane organizer proteins, respectively (32, 36, 38). Our proteomics analysis also confirmed the presence of programmed cell death 6-interacting protein (PDCD6IP) and syntenin-1 (*Sdcbp*) in purified vesicles (Tables 2 and 3). Syntenin-1 (*Sdcbp*) is a signaling protein and a biogenesis factor described as an extracellular vesicle marker in Vesiclepedia (RRID:SCR_019011). In addition, immunofluorescence for PDCD6IP revealed its presence at each stage and at higher levels during the earliest stage. PDCD6IP is a biogenesis factor for EVs, and is the most frequently reported extracellular vesicles marker (Vesiclepedia). Ezrin is another common EV marker, which is involved in plasma membrane/cytoskeleton cross-linkage during vesicle formation (39, 88); it is present in uterine fluid EVs (Table 3). The biogenesis factor, syntenin-1 (*Sdcbp*), and ezrin could be attached to EV membrane via their phosphatidylinositol 4, 5-bisphosphate–binding sites (Table 3). PDCD6IP, syntenin-1, and ezrin have been previously identified in bone and cartilage EVs (31–33).

In our previous study, we proposed a role for EDIL3 and MFGE8 in targeting vesicles containing ACC cargo to the mineralization site (27). EDIL3 and MFGE8 are the 6th and 34th most abundant eggshell proteins, respectively (71). EDIL3 was previously identified in the proteome of cartilage EVs (33). In this study, we identified EDIL3 in purified EVs (Tables 2 and 3), and demonstrated its vesicle specificity by Western blotting (Fig. 5*A*). EDIL3 is synthesized by the tubular glands of the uterus (Fig. 6) and could bind to vesicles via its phosphatidylserine-binding domain. In addition, EDIL3 was more abundant during the initiation of mineralization (5-10 h p.o., Fig. 6) when massive ACC deposits are detected (71). Concerning MFGE8, which is paralogous to EDIL3, we observe a high expression of its mRNA in RI compared with other tissues; only liver exhibits a higher mRNA level (27). MFGE8 was not detected in our proteomic analysis of EVs, although Western blotting revealed its presence in UF and to a lesser extend in EVs (Fig. 5*B*). Altogether, these results strongly suggest that EDIL3 is a key protein in EVs at the initiation stage of eggshell biomineralization, whereas an EV-specific role for MFGE8 is unlikely.

ACC stabilization

We propose two main hypotheses to explain the presence of stabilized ACC in uterine EVs, which are not mutually exclusive. First, accumulation of ACC in the interior of an EV may be

sufficient to ensure its stabilization, as reported *in vitro* for ACC nanoparticles stabilized in liposomes (89, 90). In this case, the membrane coats ACC and shields it from bulk water; reduced water content in the ACC milieu is sufficient to delay crystallization (91, 92). Under encapsulated conditions, the initial ACC remains isolated from the aqueous milieu and is observed to dehydrate to the more stable anhydrous ACC phase (90). Moreover, magnesium and phosphate ions, which are present in uterine fluid and in eggshell mineral, are also reported to enhance the stability of ACC and to delay its crystallization (91–93). Physicochemical vesicular conditions could therefore be a key element for ACC stabilization in uterine fluid EVs during eggshell biomineralization.

An alternative hypothesis incorporates additional molecules to thermodynamically stabilize the transient ACC phase (26). Indeed, previous studies have shown that organic matrix components of sea urchin spicules, coral skeleton, or mollusk shell can stabilize ACC (94–96). Moreover, ACC was observed using cryo-EM inside the vesicles of the sea urchin cells involved in spicule mineralization (59, 60). In this context, we paid particular attention to LYZ and OVA that were identified in our proteomic study (Tables 2 and 3), and were previously reported in chicken eggshell (70, 75, 77–79, 81, 97) and shown to modify calcium carbonate precipitation and calcite crystal morphology *in vitro* (98, 99). The role of LYZ in the stabilization of ACC has been explored but remains controversial. Only high concentrations of LYZ alter the morphology of calcite crystals *in vitro*, and LYZ is ineffective in the stabilization of ACC particles (99). However, metastable ACC was obtained *in vitro* in the presence of chicken egg white lysozyme C (100, 101). Lysozyme markedly decreased the average diameter of metastable ACC particles and promoted a network of associated particles that incorporated the protein into the precipitate (100). Additionally, lysozyme-ACC particles transform exclusively into the crystalline calcite polymorph (100, 101).

OVA is an abundant eggshell matrix protein, and its role in calcium carbonate formation and ACC stabilization has been investigated (98, 102–105). Calcium binds to OVA and this accumulation creates a nucleation center for mineral formation (105). Calcium ions are bound to the protein by complexation through acidic groups leading to protein rearrangement (97). The calcium cations are the starting points for the subsequent formation of ACC nuclei, which then undergo a series of phase transitions to the stable crystalline polymorphs (104). OVA stabilizes the unstable calcium carbonate phases *in vitro* (105, 106). Therefore, the presence of OVA in vesicles will contribute to the formation of metastable ACC (Table 3, Fig. 7).

We also identified about 20 additional proteins in UF EVs by proteomics (Table 2). Ovotransferrin can modify calcite crystal morphology *in vitro* at low concentrations (107). α2-Macroglobulin, another protein identified in our study (Table 2), is an egg yolk protein able to interact with low-density lipoprotein, which exhibits calcium binding properties and consequently could interact with ACC (RRID:SCR_002380) (18, 108). Ovomucin (MUC), ovomacroglobulin (ovostatin, OVST), and ovoglobulin G2 (TENP or OVOG2) are egg white proteins, whereas vitelline membrane outer layer protein (VMO1) is a protein enriched in the vitelline membrane (Table 2) (109). They were previously identified in eggshell (70, 71), but their role related to the calcification process is unknown. Clusterin is a chaperone protein previously identified in eggshell and proposed to prevent the premature aggregation and precipitation of eggshell matrix proteins during calcification (110). Aminopeptidase N and Loc 771972 (OCX25) are a protease and protease inhibitor, respectively (15, 111), which were also detected in vesicles (Table 2). Protease and protease inhibitors could potentially control the calcification process, either by degrading proteins or by modifying the processing of protein maturation (71). Prominin-1-A (PROM1), a protein involved in lipid metabolism was also present in vesicles but its role is not yet defined. Finally, nine EV proteins are partial Igs, with unknown functions in vesicles or in shell mineralization.

Conclusions

In the present study, we provide evidence for the first time in vertebrates of a vesicular transport pathway for delivery of stabilized amorphous calcium carbonate mineral particles. We used multiple approaches to confirm predictions based on this model. TEM coupled to spectroscopic analyses demonstrated several phases of EV formation at uterine cells, as well as the presence of EVs containing ACC mineral deposits in the UF. The major actors involved in this vesicular transport were organized into a comprehensive schema (Fig. 7), which incorporates EVs and constituent proteins in the process of shell mineralization. EDIL3 is a targeting protein that is proposed to address vesicles for delivery of ACC to the mineralization site. Calcium accumulation by vesicles is promoted by annexins 1, 2, and 8, whereas carbonic anhydrase 4 catalyzes bicarbonate formation from CO_2. Moreover, our study identified and characterized several additional proteins that could contribute to the stabilization of ACC inside vesicles, under favorable physical and chemical conditions.

Experimental procedures

Ethical statement and housing

All animal-handling protocols were carried out in accordance with the European Communities Council Directives concerning the practice for the care and use of animals for Scientific Purposes and the French Ministry on Animal experimentation, and were performed under the supervision of authorized scientists (authorization number 7323, delivered by the French Ministry of Education and Research). Birds were kept in the experimental unit PEAT 1295 of INRA, which has permission to rear birds and to perform euthanasia of experimental animals (decree number B37-175-1 of August 28th 2012 delivered by the "Préfécture d'Indre et Loire" following inspection by the Direction of Veterinary Services). Our experimental protocol was approved by the ethical committee "Comité d'éthique de Val de Loire, officially registered under number 19 of the French National Ethics Committee for Animal Experimentation" under agreement number 16099-015902.

Mature brown egg-laying hens (ISA-Hendrix, 40 and 90 weeks old at sampling) were kept in individual cages furnished with automatic equipment for recording of the oviposition (egg-laying) times. Animals were fed layer mash *ad libitum* and

exposed to a 14-h light/10-h darkness cycle. Following collection and removal of egg contents, the eggshells were thoroughly washed with water, air dried, and stored at −20 °C.

Tissue and uterine fluid collection

Thirty-two brown laying hens (ISA-Hendrix, 26 and 6 at 40 and 90 weeks old, respectively) were sacrificed by lethal intravenous injection of Dolethal® (Vetoquinol, Magny-vernois, France) at the initial phase of eggshell mineralization (5-7 h p.o.), the onset of the active mineralization phase (10 h p.o.), or during the linear growth phase of rapid mineralization (16-18 h p.o.).

For RT-PCR and Western blotting analyses, various tissues (duodenum, D; kidney, K; liver, L) and oviduct regions (Ma, WI, RI, and Ut) were collected from 40-week–old hens sacrificed at 10 h p.o., whereas mid-shaft tibial bones (B) were collected at 18 h p.o from 90-week–old hens. Oviduct epithelium samples were obtained by scraping the inner surface. Mid-shaft tibial bone samples were cleaned of muscle but were not flushed of marrow; duodenum tissues were directly cleaned by immersion in physiological saline. Liver was collected from the right lobe. After that, tissues were directly immersed in liquid nitrogen and then stored at −80 °C in cryo-tubes until RNA or protein extraction.

Small pieces of uterine wall (0.5 cm^2) were also sampled at 16 h p.o. from 40-week–old hens for EM, and were fixed by incubation at room temperature for 24 h in 4% paraformaldehyde, 1% glutaraldehyde in 0.1 M phosphate buffer (pH 7.3). Fixed tissues were stored at 4 °C until preparation of sections.

For immunofluorescence analysis, small pieces (2 × 0.4 cm) of the uterus at each stage (5, 6, 7, 10, and 16 h p.o.), from 25 hens at 40 weeks old, were embedded in optimal cutting temperature compound mounting medium for cryosectioning (VWR, Radnor, USA) using molds and direct immersion in isopentane cooled by liquid nitrogen. The blocks of optimal cutting temperature containing uterus pieces were stored at −80 °C until cryosectioning.

UF was collected as previously described (20). Briefly, egg expulsion was induced by injection of 50 μg of prostaglandin-F2α in the alar vein of 40-week–old hens, either at 9 or 16 h p.o. Following egg expulsion, UF was collected directly by gravity in a plastic tube placed at the entrance of the everted vagina. A portion of the fluid was promptly pipetted and deposited in liquid nitrogen to obtain 50-μl beads of uterine fluid for storage at −80 °C until use for electron microcopy. The remaining UF was diluted in PBS (PBS, 4:1, v/v) in cryotubes maintained on ice and immediately used for extracellular vesicle isolation.

mRNA levels

Total RNA was extracted from tissues harvested at 10 h p.o. (except bone, which was extracted at 18 h p.o.), and treated as previously described (27). Briefly, the concentration of each RNA sample was measured at 260 nm with NanoDrop™ and their integrity was assessed on 1.5% agarose gels. Total RNA samples (1 μg) were reverse-transcribed using RNase H-Moloney murine leukemia virus reverse transcriptase (Superscript II, Invitrogen) and Oligo(dT)™ primers (Invitrogen). Primers for the *Edil3*, *Mfge8*, *Ca4*, the 31 vesicular genes, and the eight housekeeping genes (*B2m, Eif3i, Gapdh, Gusb, Stag2, Tbp, Sdha*, and *Ppia*) were designed from *G. gallus* gene sequences (Table S3), using Primer-BLAST on National Center for Biotechnology Information (NCBI), and were synthesized (Eurogentec, Lièges, Belgium). Primer efficiencies were evaluated by RT-qPCR using LightCycler® 480 SYBR Green I Master and LightCycler® 480 instrument II (Roche, Bâle, Switzerland). mRNA level was quantified using the Biomark microfluidic system, in which every sample-gene combination were quantified using a 96.96 Dynamic Array™ IFCs (BMK-M-96.96, Fluidigm®, San Francisco, CA) at the GeT-GenoToul platform (Toulouse, France). Samples were pre-amplified according to the manufacturer's specifications. PCR was then performed using the following thermal protocols: thermal mix (50 °C, 2 min; 70 °C, 30 min; 25 °C, 10 min), hot start (50 °C, 2 min; 95 °C, 10 min), 35 PCR cycles (95 °C, 15 s; 60 °C, 60 s), and melting analysis (60 °C, 30 s; 95 °C, 1 °C/3 s). Real time-quantitative PCR results were analyzed using Fluidigm Real-time PCR analysis software version 4.1.3 (RRID:SCR_015686). Six biological replicates and two technical replicates were carried out for each tissue. GenNorm software (RRID:SCR_006763) was used for validation of housekeeping gene stability. The normalized quantities were calculated using the following formula: (gene $efficiency^{(ctcalibrator-ctsample)}$)/geometric average quantity of the eight housekeeping genes. Normalized quantities were compared between various measured tissues and oviduct segments using one-way ANOVA followed by Tukey pairwise test analysis on Minitab® 18 software (RRID:SCR_014483). A p value <0.05 was selected as the threshold for significance between different groups. The heat map of the mRNA levels (Row-Z score) in different tissues for *Edil3*, *Mfge8,* and the 31 vesicular genes was computed using the heatmap.2 function from gplots packages of Rstudio software 1.1.456 (RRID:SCR_000432). Row and column clustering were performed using Pearson-ward.D2 methods and Spearman-Ward.D2 methods, respectively.

The *Ca4* mRNA was amplified by end point PCR in each oviduct segment and tissues using DreamTaq PCR Master Mix 2 × (ThermoFisher Scientific, Waltham, MA) and Mastercycler gradient (Eppendorf, Hamburg, Germany). After 3 min of denaturation, 35 cycles were used (95 °C, 30 s; 60 °C, 30 s; 72 °C, 30 s) to amplify PCR products, followed by a final elongation for 15 min. PCR products were then mixed with Trackit cyan/orange Loading buffer 6 times (ThermoFisher Scientific), loaded on a 2.5% agarose gel, and migrated for 30 min at 100 V using the Mupid-One electrophoresis system (Dominique Dutscher, Issy-les-mouligneaux, France). The Trackit 100-bp DNA ladder was used (ThermoFisher Scientific) to determine the size of PCR products. Imaging was performed using the Syngene GeneGenius Gel Light Imaging System (Syngene, Cambridge, UK).

Extracellular vesicle isolation from uterine fluid and extraction of soluble eggshell matrix proteins

EVs were isolated from uterine fluid harvested at 9 and 16 h p.o., using previously described methodology (112). Briefly, UF

diluted in PBS was centrifuged at 100 × *g* for 15 min and then at 12,000 × *g* for 15 min to remove cell debris. Two successive ultracentrifugation steps at 100,000 × *g* (Beckman Coulter L8-70M, Beckman Coulter, Brea, CA) were then performed during 90 min to pellet the EVs. Aliquots of the supernatants corresponding to UF without EVs were sampled and stored at −20 °C. The pellet was suspended in 50 μl of PBS and stored at −20 °C until TEM, nanoLC-MS/MS, and Western blotting analysis.

SEP from normally laid eggs were extracted as previously detailed (107). Briefly, eggshell pieces with eggshell membranes were immersed in 154 mM NaCl containing protease inhibitors (2.5 mM benzamidine-HCl, 50 mM ϵ-amino-*n*-caproic acid, 0.5 mM *N*-ethymaleimide, and 1 mM phenylmethylsulfonyl fluoride), and then ground into a fine powder. Eggshell powders were fully demineralized by immersion in 20% acetic acid, and the resulting suspensions were dialyzed (cutoff 3,500 Da; dialysis membrane Spectra/Por™, ThermoFisher Scientific) against demineralized water for 24 h at 4 °C and lyophilized. Powdered samples were incubated overnight at 4 °C in 4 M guanidine-HCl, 5 mM benzamidine-HCl, 0.1 M ϵ-amino-*n*-caproic acid, 10 mM EDTA, 50 mM sodium acetate, and 1 mM phenylmethylsulfonyl fluoride, and then dialyzed (cutoff 3, 500 Da) against 0.5 M sodium acetate (pH 7.4) for 24 h at 4 °C, followed by centrifugation at 2, 000 × *g* for 10 min at 4 °C. The resulting SEP (supernatants) were stored at −20°C.

Electrophoresis and Western blotting analyses

Protein concentrations were determined using the Bio-Rad DC Protein Assay kit II (Bio-Rad, Marnes-la Coquette, France) in accordance with manufacturer's instructions and using BSA (Sigma-Aldrich, Saint-Quentin Fallavier, France) as standard. Fifteen micrograms of each sample were diluted into Laemmli sample buffer (51, v/v) and boiled for 5 min. Protein samples were then separated on 12% polyacrylamide gels (Mini-Protean II electrophoresis cell, Bio-Rad, Marnes-la-Coquette, France) and transferred to 0.2 μM nitrocellulose blotting membrane (GE Healthcare, Little Chalfont, UK) for Western blotting analysis. Briefly, membranes were washed 5 min in TBS (50 mM Tris-HCl, 150 mM NaCl, pH 7.4), blocked with the Odyssey® blocking buffer (LI-COR, Bad Homburg, Germany) in TBS (1:1, v/v), and then incubated for 3 h in the blocking solution (Odyssey® blocking buffer/TBS, 1:1, v/v) containing 0.1% Tween-20 and anti-EDIL3 (1:1,000) or anti-MFGE8 antibodies (1:1,000) (Table S4). Membranes were sequentially washed for 5 min in TBS, 0.1% Tween-20, and then incubated for 1 h in the blocking solution containing 0.1% Tween-20 and AlexaFluor® 680 goat anti-rabbit (H + L) secondary antibody (1:20,000; ThermoFisher Scientific) (Table S4). Finally, membranes were washed three times in TBS containing 0.1% Tween-20 and twice in TBS. Immunoreactive bands were revealed using the Odyssey® imaging system (LI-COR, Bad Homburg, Germany) at 700 nm.

Immunofluorescence of uterine tissue

Serial sections (10 μM) were prepared from uterus embedded in optimal cutting temperature (harvested at 5, 6, 7, 10, and 16 h p.o.) using the CM3050 S cryostat (Leica, Wetzlar, Germany). Sections (stored at −80 °C until use) were thawed for 30 min at room temperature and rehydrated during 5 min in 1× PBS before immunolabeling. The blocking step was performed with 1× PBS, 3% BSA for 20 min at room temperature. Sections were then incubated in 1× PBS, 3% BSA with diluted primary antibodies (anti-ANXA1, anti-ANXA2, anti-ANXA8, anti-CA4, anti-EDIL3, or anti-PDCD6IP, Table S4). Sections were washed 3 times at room temperature for 5 min in 1× PBS. Negative controls were prepared without primary antibody. Sections were washed 3 times for 5 min at room temperature in 1× PBS. Then, according to the primary antibody, sections were incubated with either goat anti-rabbit secondary antibody (IgG, H + L), AlexaFluor® 488 (1:1,000; ThermoFisher Scientific) or goat anti-mouse IgG1 cross-adsorbed secondary antibody, AlexaFluor® 555 (1:1,000; ThermoFisher Scientific) (Table S4) in 1× PBS, 1% BSA for 1 h at room temperature. All immunolabeling was performed on duplicate sections. Sections were washed three times for 5 min at room temperature and then mounted using Fluoroshield™ with 4′,6-diamidino-2-phenylindole histology mounting medium (Sigma-Aldrich, Saint-Quentin Fallavier, France). Sections were observed with Axioplan II Fluorescence Microscope (Zeiss, Oberkochen, Germany) and images were acquired using an INFINITY microscope camera (Lumenera, Nepean, Canada).

Proteomics analysis of uterine fluid extracellular vesicles

Sixty micrograms of purified EVs resuspended in PBS were diluted into 2% SDS Laemmli sample buffer (5:1, v/v) and boiled for 5 min. EV proteins were electrophoresed on a 12.5% polyacrylamide gel (50 V, 30 min) to obtain a single band (Mini-Protean II electrophoresis cell, Bio-Rad, Marnes-la-Coquette, France). The gel was stained with Coomassie Blue and the single band of proteins was excised and subjected to in-gel digestion with bovine trypsin (Roche Diagnostics GmbH, Mannheim, Germany) as previously described by Marie *et al.* (84) for analysis by nanoscale liquid chromatography–tandem MS (nanoLC–MS/MS). MS/MS ion searches were performed using Mascot search engine version 2.6 (Matrix Science, London, UK) via Proteome Discoverer 2.1 software (ThermoFisher Scientific, Bremen, Germany) against the NCBIprot_chordata database (July 2018). The search parameters included trypsin as a protease with two allowed missed cleavages, carbamidomethylcysteine, methionine oxidation, and acetylation of protein N termini as variable modifications. The tolerance of the ions was set to 5 ppm for parent and 0.8 Da for fragment ion matches. Mascot results obtained from the target and decoy databases searches were subjected to Scaffold software (version 4.8.8, Proteome Software, Portland, OR) using the protein cluster analysis option (assemblage of proteins into clusters based on shared peptide evidence). Peptide and protein identifications were accepted if they could be established at greater than 95.0% probability as specified by the Peptide Prophet algorithm and by the Protein Prophet algorithm, respectively. Protein identifications were accepted if they contained at least two identified peptides.

Transmission EM and electron energy loss spectroscopy analyses of uterine fluid

Frozen beads of UF harvested at 16 h p.o. were deposited on copper TEM grids and dried for 1 min. Excess UF was then absorbed with filter paper and the grid was immediately observed with the TEM-ZEISS LIBRA 120 instrument (ZEISS, Oberkochen, Germany). EVs were localized under the TEM and EELS spectra from 270 to 410 eV and from 460 to 600 eV were acquired (Table S1). Mapping of elemental calcium (345-355 eV) and carbon (280-290 eV) were performed to determine the spatial distribution of $CaCO_3$ and organic carbon in EVs.

Transmission EM and energy-dispersive X-ray spectroscopy analyses of uterus and uterine fluid

Fixed pieces of uterus were washed in PBS and post-fixed by incubation with 2% osmium tetroxide for 1 h. Samples were then fully dehydrated in a graded series of ethanol solutions and embedded in Epon resin, which was polymerized by heating from 37 to 60 °C. Ultra-thin sections (50–70 nm thick) of these blocks were obtained with a LEICA Ultracut UCT ultramicrotome (Leica, Wetzlar, Germany). Sections were stained with 5% uranyl acetate, 5% lead citrate, and observations were made with a TEM-1400 Plus electron microscope (JEOL, Tokyo, Japan).

UF harvested at 16 h p.o. and stored as frozen beads was deposited on a TEM grids (C coated) and then dried for 1 min. Excess UF was then absorbed with filter paper, stained with uranyl acetate 2%, and the grid was immediately observed with a TEM-1400 Plus electron microscope (JEOL, Tokyo, Japan). EVs were observed under the TEM (BF/DF detector) and EDS (Oxford 65 mm^2 detector) analysis was performed on EVs to detect elemental calcium, carbon, and oxygen (AZtec software). SAED patterns were registered to determine the crystallinity of mineral deposits observed wthin EVs.

Data availability

All data are contained within the manuscript.

Acknowledgments—We are grateful to the experimental unit (PEAT, INRAE, 2018, Poultry Experimental Facility) for the care of birds, the GeT-GenoToul platform Toulouse for performing real time-quantitative PCR with the Biomark Fluidigm system, and Centro de Instrumentación Científica de la Universidad de Granada for electron microscopy and spectroscopic analysis. We acknowledge Pierre-Ivan Raynal and Sonia Georgeault from the IBiSA electron microscopy platform of the "Université François Rabelais" of Tours for their assistance. We also acknowledge Nadine Gérard, Cindy Riou, and Agostinho Alcantara-Neto from UMR "Physiologie de la Reproduction et des Comportements" (INRAE Centre Val de Loire) for their help in extracellular vesicle isolation.

Author contributions—L. S., N. L. R., M. T. H., and J. G. conceptualization; L. S., J. E., A. B. R.-N., V. L., and L. C.-S. resources; L. S., J. E., A. B. R.-N., V. L., L. C.-S., and M. T. H. formal analysis; L. S., N. L. R., J. E., and J. G. supervision; L. S. and J. G. funding acquisition; L. S., N. L. R., J. E., A. B. R.-N., V. L., L. C.-S., M. T. H., and J. G. validation; L. S., N. L. R., J. E., A. B. R.-N., V. L., L. C.-S., M. T. H., and J. G. investigation; L. S. and J. G. visualization; L. S., N. L. R., J. E., A. B. R.-N., V. L., L. C.-S., M. T. H., and J. G. methodology; L. S. writing-original draft; L. S. and J. G. project administration; L. S., N. L. R., J. E., A. B. R.-N., V. L., L. C.-S., M. T. H., and J. G. writing-review and editing; V. L. and L. C.-S. software.

Funding and additional information—This work was supported by the Université François Rabelais de Tours and the Région Centre Val de Loire (to L. S.), NSERC Grant RGPIN-2016-04410 and Le STUDIUM and is a Le STUDIUM Research Fellow, Loire Valley Institute for Advanced Studies, Orleans-Tours, and BOA, INRAE, Centre Val de Loire, Nouzilly, France (to M. T. H.).

Conflict of interest—The authors declare that they have no conflicts of interest with the contents of this article.

Abbreviations—The abbreviations used are: ACC, amorphous calcium carbonate; B, bone; $CaCO_3$, calcium carbonate; D, duodenum; EDS, energy-dispersive X-ray spectroscopy; EELS, electron energy loss spectroscopy; EV, extracellular vesicle; K, kidney; L, liver; Ma, magnum; p.o., post-ovulation; RI, red isthmus; SAED, selected area electron diffraction; SEP, soluble eggshell proteins; SST, sperm storage tubules; TBS, Tris-buffered saline; TEM, transmission electron microscopy; UF, uterine fluid; Ut, uterus; WI, white isthmus; ACE, angiotensin-converting enzyme precursor; PDCD6IP, programmed cell death 6-interacting protein; ANOVA, analysis of variance; EGF, epidermal growth factor; EDX, energy-dispersive X-ray spectroscopy; EDIL3, EGF-like repeat and discoidin I-like domain-containing protein 3; EZR, ezrin; LYZ, lysozyme C; OVA, ovalbumin; CA4, carbonic anhydrase-4.

References

1. Lowenstam, H. A., and Weiner, S. (1989) *On Biomineralization*, Oxford University Press, New York
2. Ziegler, A. (1994) Ultrastructure and electron spectroscopic diffraction analysis of the sternal calcium deposits of *Porcellio scaber* Latr (isopoda, crustacea). *J. Struct. Biol.* **112,** 110–116 CrossRef
3. Brečević, L., and Nielsen, A. E. (1989) Solubility of amorphous calcium-carbonate. *J. Crystal Growth* **98,** 504–510 CrossRef
4. Addadi, L., Raz, S., and Weiner, S. (2003) Taking advantage of disorder: Amorphous calcium carbonate and its roles in biomineralization. *Adv. Materials* **15,** 959–970 CrossRef
5. Aizenberg, J., Lambert, G., Weiner, S., and Addadi, L. (2002) Factors involved in the formation of amorphous and crystalline calcium carbonate: a study of an ascidian skeleton. *J. Am. Chem. Soc.* **124,** 32–39 CrossRef Medline
6. Beniash, E., Addadi, L., and Weiner, S. (1999) Cellular control over spicule formation in sea urchin embryos: a structural approach. *J. Struct. Biol.* **125,** 50–62 CrossRef Medline
7. Addadi, L., Joester, D., Nudelman, F., and Weiner, S. (2006) Mollusk shell formation: a source of new concepts for understanding biomineralization processes. *Chemistry* **12,** 980–987 CrossRef Medline
8. Bahn, S. Y., Jo, B. H., Choi, Y. S., and Cha, H. J. (2017) Control of nacre biomineralization by Pif80 in pearl oyster. *Sci. Adv.* **3,** e1700765 CrossRef
9. Mass, T., Giuffre, A. J., Sun, C. Y., Stifler, C. A., Frazier, M. J., Neder, M., Tamura, N., Stan, C. V., Marcus, M. A., and Gilbert, P. (2017) Amorphous calcium carbonate particles form coral skeletons. *Proc. Natl. Acad. Sci. U.S.A.* **114,** E7670–E7678 CrossRef Medline
10. Weiner, S., and Dove, P. M. (2003) An overview of biomineralization processes and the problem of the vital effect. *Biomineralization* **54,** 1–29 CrossRef

11. Levi-Kalisman, Y., Raz, S., Weiner, S., Addadi, L., and Sagi, I. (2002) Structural differences between biogenic amorphous calcium carbonate phases using X-ray absorption spectroscopy. *Adv. Funct. Materials* **12,** 43–48 CrossRef
12. Claramunt, S., and Cracraft, J. (2015) A new time tree reveals Earth history's imprint on the evolution of modern birds. *Sci. Adv.* **1,** e1501005 CrossRef
13. Hincke, M. T., Da Silva, M., Guyot, N., Gautron, J., McKee, M. D., Guabiraba-Brito, R., and Réhault-Godbert, S. (2019) Dynamics of structural barriers and innate immune components during incubation of the avian egg: critical interplay between autonomous embryonic development and maternal anticipation. *J. Innate Immun.* **11,** 111–124 CrossRef Medline
14. Nys, Y., Hincke, M. T., Arias, J. L., Garcia-Ruiz, J. M., and Solomon, S. E. (1999) Avian eggshell mineralization. *Poultry Avian Biol. Rev.* **10,** 143–166
15. Nys, Y., Hincke, M. T., Hernandez-Hernandez, A., Rodriguez-Navarro, A. B., Gomez-Morales, J., Jonchere, V., Garcia-Ruiz, J. M., and Gautron, J. (2011) Eggshell ultrastructure, properties and the process of mineralization: involvement of organic matrix in the eggshell fabric. *Productions Animales* **23,** 143–154 CrossRef
16. Arias, J. L., Fink, D. J., Xiao, S. Q., Heuer, A. H., and Caplan, A. I. (1993) Biomineralization and eggshells: cell-mediated acellular compartments of mineralized extracellular matrix. *Int. Rev. Cytol.* **145,** 217–250 CrossRef Medline
17. Nys, Y., Gautron, J., Garcia-Ruiz, J. M., and Hincke, M. T. (2004) Avian eggshell mineralization: biochemical and functional characterization of matrix proteins. *Comptes Rendus Palevol.* **3,** 549–562 CrossRef
18. Nys, Y., and Guyot, N. (2011) Egg formation and chemistry. In *Improving the Safety and Quality of Eggs and Egg Products* (Nys, Y., Bain, M., and Van Immerseel, F., eds) pp. 83–132, Woodhead Publishing, Cambridge
19. Nys, Y., and Gautron, J. (2007) Structure and formation of the eggshell. In *Bioactive Egg Compounds* (Huopalahti, R., López-Fandiño, R., Anton, M., and Schade, R., eds) pp. 99–102, Springer, Berlin
20. Gautron, J., Hincke, M. T., and Nys, Y. (1997) Precursor matrix proteins in the uterine fluid change with stages of eggshell formation in hens. *Connect. Tissue Res.* **36,** 195–210 CrossRef Medline
21. Jonchère, V., Brionne, A., Gautron, J., and Nys, Y. (2012) Identification of uterine ion transporters for mineralisation precursors of the avian eggshell. *BMC Physiol.* **12,** 10 CrossRef Medline
22. Jonchère, V., Réhault-Godbert, S., Hennequet-Antier, C., Cabau, C., Sibut, V., Cogburn, L. A., Nys, Y., and Gautron, J. (2010) Gene expression profiling to identify eggshell proteins involved in physical defense of the chicken egg. *BMC Genomics* **11,** 57 CrossRef Medline
23. Hincke, M. T., Nys, Y., Gautron, J., Mann, K., Rodriguez-Navarro, A. B., and McKee, M. D. (2012) The eggshell: structure, composition and mineralization. *Front. Biosci.* **17,** 1266–1280 CrossRef Medline
24. Nys, Y., and Le Roy, N. (2018) Calcium homeostasis and eggshell biomineralization in female chicken. In *Vitamin D* (Feldman, D., ed) 4 Ed., pp. 361–382, Academic Press, Cambridge
25. Brionne, A., Nys, Y., Hennequet-Antier, C., and Gautron, J. (2014) Hen uterine gene expression profiling during eggshell formation reveals putative proteins involved in the supply of minerals or in the shell mineralization process. *BMC Genomics* **15,** 220 CrossRef Medline
26. Rodríguez-Navarro, A. B., Marie, P., Nys, Y., Hincke, M. T., and Gautron, J. (2015) Amorphous calcium carbonate controls avian eggshell mineralization: a new paradigm for understanding rapid eggshell calcification. *J. Struct. Biol.* **190,** 291–303 CrossRef Medline
27. Stapane, L., Le Roy, N., Hincke, M. T., and Gautron, J. (2019) The glycoproteins EDIL3 and MFGE8 regulate vesicle-mediated eggshell calcification in a new model for avian biomineralization. *J. Biol. Chem.* **294,** 14526–14545 CrossRef Medline
28. DeVol, R. T., Metzler, R. A., Kabalah-Amitai, L., Pokroy, B., Politi, Y., Gal, A., Addadi, L., Weiner, S., Fernandez-Martinez, A., Demichelis, R., Gale, J. D., Ihli, J., Meldrum, F. C., Blonsky, A. Z., Killian, C. E., *et al.* (2014) Oxygen spectroscopy and polarization-dependent imaging contrast (PIC)-mapping of calcium carbonate minerals and biominerals. *J. Phys. Chem. B* **118,** 8449–8457 CrossRef Medline
29. Garvie, L. A. J., Craven, A. J., and Brydson, R. (1995) Use of electron-energy-loss near-edge fine-structure in the study of minerals. *Am. Mineralogist* **80,** 1132–1425 CrossRef
30. Macías-Sánchez, E., Willinger, M. G., Pina, C. M., and Checa, A. G. (2017) Transformation of ACC into aragonite and the origin of the nanogranular structure of nacre. *Sci. Rep.* **7** CrossRef
31. Balcerzak, M., Malinowska, A., Thouverey, C., Sekrecka, A., Dadlez, M., Buchet, R., and Pikula, S. (2008) Proteome analysis of matrix vesicles isolated from femurs of chicken embryo. *Proteomics* **8,** 192–205 CrossRef Medline
32. Shapiro, I. M., Landis, W. J., and Risbud, M. V. (2015) Matrix vesicles: are they anchored exosomes? *Bone* **79,** 29–36 CrossRef Medline
33. Rosenthal, A. K., Gohr, C. M., Ninomiya, J., and Wakim, B. T. (2011) Proteomic analysis of articular cartilage vesicles from normal and osteoarthritic cartilage. *Arthritis Rheum.* **63,** 401–411 CrossRef
34. Thouverey, C., Malinowska, A., Balcerzak, M., Strzelecka-Kiliszek, A., Buchet, R., Dadlez, M., and Pikula, S. (2011) Proteomic characterization of biogenesis and functions of matrix vesicles released from mineralizing human osteoblast-like cells. *J. Proteomics* **74,** 1123–1134 CrossRef Medline
35. Colombo, M., Raposo, G., and Théry, C. (2014) Biogenesis, secretion, and intercellular interactions of exosomes and other extracellular vesicles. *Annu. Rev. Cell Dev. Biol.* **30,** 255–289 CrossRef Medline
36. Azoidis, I., Cox, S. C., and Davies, O. G. (2018) The role of extracellular vesicles in biomineralisation: current perspective and application in regenerative medicine. *J. Tissue Eng.* **9,** 2041731418810130 CrossRef Medline
37. Hessvik, N. P., and Llorente, A. (2018) Current knowledge on exosome biogenesis and release. *Cell. Mol. Life Sci.* **75,** 193–208 CrossRef Medline
38. Van Niel, G., D'Angelo, G., and Raposo, G. (2018) Shedding light on the cell biology of extracellular vesicles. *Nat. Rev. Mol. Cell Biol.* **19,** 213–228 CrossRef Medline
39. Pathan, M., Fonseka, P., Chitti, S. V., Kang, T., Sanwlani, R., Van Deun, J., Hendrix, A., and Mathivanan, S. (2019) Vesiclepedia 2019: a compendium of RNA, proteins, lipids and metabolites in extracellular vesicles. *Nucleic Acids Res.* **47,** D516–D519 CrossRef Medline
40. Hasegawa, T., Yamamoto, T., Tsuchiya, E., Hongo, H., Tsuboi, K., Kudo, A., Abe, M., Yoshida, T., Nagai, T., Khadiza, N., Yokoyama, A., Oda, K., Ozawa, H., de Freitas, P. H. L., Li, M., *et al.* (2017) Ultrastructural and biochemical aspects of matrix vesicle-mediated mineralization. *Jpn. Dent. Sci. Rev.* **53,** 34–45 CrossRef Medline
41. Golub, E. E. (2009) Role of matrix vesicles in biomineralization. *Biochim. Biophys. Acta* **1790,** 1592–1598 CrossRef Medline
42. Kalra, H., Drummen, G. P. C., and Mathivanan, S. (2016) Focus on extracellular vesicles: introducing the next small big thing. *Int. J. Mol. Sci.* **17,** 170 CrossRefMedline
43. Barreiro, K., and Holthofer, H. (2017) Urinary extracellular vesicles: a promising shortcut to novel biomarker discoveries. *Cell Tissue Res.* **369,** 217–227 CrossRef Medline
44. Basso, M., and Bonetto, V. (2016) Extracellular vesicles and a novel form of communication in the brain. *Front. Neurosci.* **10,** 127 CrossRef
45. Gho, Y. S., and Lee, C. (2017) Emergent properties of extracellular vesicles: a holistic approach to decode the complexity of intercellular communication networks. *Mol. Biosystems* **13,** 1291–1296 CrossRef Medline
46. Gho, Y. S., and Lee, J. (2019) Special issue on the role of extracellular vesicles in human diseases. *Exp. Mol. Med.* **51,** 1–2 CrossRef Medline
47. Kim, C. W., Lee, H. M., Lee, T. H., Kang, C. H., Kleinman, H. K., and Gho, Y. S. (2002) Extracellular membrane vesicles from tumor cells promote angiogenesis via sphingomyelin. *Cancer Res.* **62,** 6312–6317 Medline
48. Pomatto, M. A. C., Gai, C., Bussolati, B., and Camussi, G. (2017) Extracellular vesicles in renal pathophysiology. *Front. Mol. Biosci.* **4,** 37 CrossRefMedline
49. Riou, C., Brionne, A., Cordeiro, L., Harichaux, G., Gargaros, A., Labas, V., Gautron, J., and Gérard, N. (2020) Avian uterine fluid proteome: exosomes and biological processes potentially involved in sperm survival. *Mol. Reprod. Dev.* **87,** 454–470 CrossRef Medline

50. Bottini, M., Mebarek, S., Anderson, K. L., Strzelecka-Kiliszek, A., Bozycki, L., Simão, A. M. S., Bolean, M., Ciancaglini, P., Pikula, J. B., Pikula, S., Magne, D., Volkmann, N., Hanein, D., Millán, J. L., and Buchet, R. (2018) Matrix vesicles from chondrocytes and osteoblasts: their biogenesis, properties, functions and biomimetic models. *Biochim. Biophys. Acta* **1862,** 532–546 CrossRef Medline
51. Weiner, S., and Addadi, L. (2011) Crystallization pathways in biomineralization. *Annu. Rev. Materials Res.* **41,** 21–40 CrossRef
52. Gloux, A., Le Roy, N., Brionne, A., Bonin, E., Juanchich, A., Benzoni, G., Piketty, M. L., Prié, D., Nys, Y., Gautron, J., Narcy, A., and Duclos, M. J. (2019) Candidate genes of the transcellular and paracellular calcium absorption pathways in the small intestine of laying hens. *Poultry Sci.* **98,** 6005–6018 CrossRef Medline
53. Nys, Y., Zawadzki, J., Gautron, J., and Mills, A. D. (1991) Whitening of brown-shelled eggs: mineral composition of uterine fluid and rate of protoporphyrin deposition. *Poultry Sci.* **70,** 1236–1245 CrossRef Medline
54. Waqas, M. Y., Yang, P., Ahmed, N., Zhang, Q., Liu, T., Li, Q., Hu, L., Hong, C., and Chen, Q. (2016) Characterization of the ultrastructure in the uterovaginal junction of the hen. *Poultry Sci.* **95,** 2112–2119 CrossRef Medline
55. Chien, Y. C., Hincke, M. T., and McKee, M. D. (2009) Ultrastructure of avian eggshell during resorption following egg fertilization. *J. Struct. Biol.* **168,** 527–538 CrossRef Medline
56. Hincke, M. T., Nys, Y., and Gautron, J. (2010) The role of matrix proteins in eggshell formation. *J. Poultry Sci.* **47,** 208–219 CrossRef
57. Gautron, J., and Nys, Y. (2007) Function of eggshell matrix proteins. In *Bioactive Egg Compounds* (Huopalahti, R., López-Fandiño, R., Anton, M., and Schade, R., eds) pp. 109–115, Springer, Berlin
58. Gautron, J. (2019) Proteomics analysis of avian eggshell matrix proteins: toward new advances on biomineralization. *Proteomics* **19,** 1900120 CrossRef
59. Vidavsky, N., Addadi, S., Mahamid, J., Shimoni, E., Ben-Ezra, D., Shpigel, M., Weiner, S., and Addadi, L. (2014) Initial stages of calcium uptake and mineral deposition in sea urchin embryos. *Proc. Natl. Acad. Sci. U.S.A.* **111,** 39–44 CrossRef Medline
60. Vidavsky, N., Masic, A., Schertel, A., Weiner, S., and Addadi, L. (2015) Mineral-bearing vesicle transport in sea urchin embryos. *J. Struct. Biol.* **192,** 358–365 CrossRef Medline
61. Mahamid, J., Sharir, A., Gur, D., Zelzer, E., Addadi, L., and Weiner, S. (2011) Bone mineralization proceeds through intracellular calcium phosphate loaded vesicles: a cryo-electron microscopy study. *J. Struct. Biol.* **174**, 527–535 CrossRef Medline
62. Gay, C. V., Schraer, H., and Hargest, T. E. (1978) Ultrastructure of matrix vesicles and mineral in unfixed embryonic bone. *Metab. Bone Dis. Relat. Res.* **1,** 105–108 CrossRef
63. Wu, L. N., Yoshimori, T., Genge, B. R., Sauer, G. R., Kirsch, T., Ishikawa, Y., and Wuthier, R. E. (1993) Characterization of the nucleational core complex responsible for mineral induction by growth plate cartilage matrix vesicles. *J. Biol. Chem.* **268,** 25084–25094 Medline
64. Anderson, H. C., Garimella, R., and Tague, S. E. (2005) The role of matrix vesicles in growth plate development and biomineralization. *Front. Biosci.* **10,** 822–837 CrossRef
65. Khalifa, G., Kahil, K., Addadi, L., and Weiner, S. (2018) Calcium ion and mineral pathways in biomineralization: a perspective. In *Biomineralization: from Molecular and Nano-structural Analyses to Environmental Science* (Endo, K., Kogure, T., and Nagasawa, H., eds) pp. 97–103, Springer, Singapore
66. Rojas, E., Arispe, N., Haigler, H. T., Burns, A. L., and Pollard, H. B. (1992) Identification of annexins as calcium channels in biological-membranes. *Bone Miner.* **17,** 214–218 CrossRef Medline
67. Wuthier, R. E., and Lipscomb, G. F. (2011) Matrix vesicles: structure, composition, formation and function in calcification. *Front. Bioscience (Landmark)* **16,** 2812–2902 CrossRef Medline
68. Cao, X., Genge, B. R., Wu, L. N., Buzzi, W. R., Showman, R. M., and Wuthier, R. E. (1993) Characterization, cloning and expression of the 67-kDa annexin from chicken growth plate cartilage matrix vesicles. *Biochem. Biophys. Res. Commun.* **197,** 556–561 CrossRef Medline
69. Arispe, N., Rojas, E., Genge, B. R., Wu, L. N., and Wuthier, R. E. (1996) Similarity in calcium channel activity of annexin V and matrix vesicles in planar lipid bilayers. *Biophys. J.* **71,** 1764–1775 CrossRef Medline
70. Mann, K., Macek, B., and Olsen, J. V. (2006) Proteomic analysis of the acid-soluble organic matrix of the chicken calcified eggshell layer. *Proteomics* **6,** 3801–3810 CrossRef Medline
71. Marie, P., Labas, V., Brionne, A., Harichaux, G., Hennequet-Antier, C., Rodriguez-Navarro, A. B., Nys, Y., and Gautron, J. (2015) Quantitative proteomics provides new insights into chicken eggshell matrix protein functions during the primary events of mineralisation and the active calcification phase. *J. Proteomics* **126,** 140–154 CrossRef Medline
72. Sun, C., Xu, G., and Yang, N. (2013) Differential label-free quantitative proteomic analysis of avian eggshell matrix and uterine fluid proteins associated with eggshell mechanical property. *Proteomics* **13,** 3523–3536 CrossRef Medline
73. Cordeiro, C. M. M., and Hincke, M. T. (2016) Quantitative proteomics analysis of eggshell membrane proteins during chick embryonic development. *J. Proteomics* **130,** 11–25 CrossRef Medline
74. Gerke, V., and Moss, S. E. (2002) Annexins: from structure to function. *Physiol. Rev.* **82,** 331–371 CrossRef Medline
75. Rose-Martel, M., Smiley, S., and Hincke, M. T. (2015) Novel identification of matrix proteins involved in calcitic biomineralization. *J. Proteomics* **116,** 81–96 CrossRef Medline
76. Hassan, M. I., Shajee, B., Waheed, A., Ahmad, F., and Sly, W. S. (2013) Structure, function and applications of carbonic anhydrase isozymes. *Bioorg. Med. Chem.* **21,** 1570–1582 CrossRef Medline
77. Rose-Martel, M., Du, J. W., and Hincke, M. T. (2012) Proteomic analysis provides new insight into the chicken eggshell cuticle. *J. Proteomics* **75,** 2697–2706 CrossRef Medline
78. Kaweewong, K., Garnjanagoonchorn, W., Jirapakkul, W., and Roytrakul, S. (2013) Solubilization and identification of hen eggshell membrane proteins during different times of chicken embryo development using the proteomic approach. *Protein J.* **32,** 297–308 CrossRef Medline
79. Mikšík, I., Sedláková, P., Lacinová, K., Pataridis, S., and Eckhardt, A. (2010) Determination of insoluble avian eggshell matrix proteins. *Anal. Bioanal. Chem.* **397,** 205–214 CrossRef Medline
80. Mann, K., and Mann, M. (2013) The proteome of the calcified layer organic matrix of turkey (*Meleagris gallopavo*) eggshell. *Proteome Sci.* **11,** 40 CrossRef Medline
81. Mikšík, I., Ergang, P., and Pácha, J. (2014) Proteomic analysis of chicken eggshell cuticle membrane layer. *Anal. Bioanal. Chem.* **406,** 7633–7640 CrossRef Medline
82. Mann, K. (2015) The calcified eggshell matrix proteome of a songbird, the zebra finch (*Taeniopygia guttata*). *Proteome Sci.* **13,** 29 CrossRef Medline
83. Mann, K., and Mann, M. (2015) Proteomic analysis of quail calcified eggshell matrix: a comparison to chicken and turkey eggshell proteomes. *Proteome Sci.* **13,** 22 CrossRef Medline
84. Marie, P., Labas, V., Brionne, A., Harichaux, G., Hennequet-Antier, C., Nys, Y., and Gautron, J. (2015) Quantitative proteomics and bioinformatic analysis provide new insight into protein function during avian eggshell biomineralization. *J. Proteomics* **113,** 178–193 CrossRef Medline
85. Ahmed, T. A., Suso, H. P., and Hincke, M. T. (2017) In-depth comparative analysis of the chicken eggshell membrane proteome. *J. Proteomics* **155,** 49–62 CrossRef Medline
86. Zhu, F., Zhang, F., Hincke, M., Yin, Z. T., Chen, S. R., Yang, N., and Hou, Z. C. (2019) iTRAQ-based quantitative proteomic analysis of duck eggshell during biomineralization. *Proteomics* **19,** e1900011 CrossRef Medline
87. Xiao, Z., Camalier, C. E., Nagashima, K., Chan, K. C., Lucas, D. A., de la Cruz, M. J., Gignac, M., Lockett, S., Issaq, H. J., Veenstra, T. D., Conrads, T. P., and Beck, G. R., Jr. (2007) Analysis of the extracellular matrix vesicle proteome in mineralizing osteoblasts. *J. Cell. Physiol.* **210,** 325–335 CrossRef Medline
88. Blin, G., Margeat, E., Carvalho, K., Royer, C. A., Roy, C., and Picart, C. (2008) Quantitative analysis of the binding of ezrin to large unilamellar vesicles containing phosphatidylinositol 4,5-bisphosphate. *Biophys. J.* **94,** 1021–1033 CrossRef Medline

89. Tester, C. C., Brock, R. E., Wu, C. H., Krejci, M. R., Weigand, S., and Joester, D. (2011) *In vitro* synthesis and stabilization of amorphous calcium carbonate (ACC) nanoparticles within liposomes. *Crystengcomm* **13,** 3975–3978 CrossRef
90. Ihli, J., Wong, W. C., Noel, E. H., Kim, Y. Y., Kulak, A. N., Christenson, H. K., Duer, M. J., and Meldrum, F. C. (2014) Dehydration and crystallization of amorphous calcium carbonate in solution and in air. *Nat. Commun.* **5,** 3169 CrossRef
91. Albéric, M., Bertinetti, L., Zou, Z. Y., Fratzl, P., Habraken, W., and Politi, Y. (2018) The crystallization of amorphous calcium carbonate is kinetically governed by ion impurities and water. *Adv. Sci.* **5,** 1701000 CrossRef Medline
92. Konrad, F., Purgstaller, B., Gallien, F., Mavromatis, V., Gane, P., and Dietzel, M. (2018) Influence of aqueous Mg concentration on the transformation of amorphous calcium carbonate. *J. Crystal Growth* **498,** 381–390 CrossRef
93. Rodriguez-Blanco, J. D., Shaw, S., Bots, P., Roncal-Herrero, T., and Benning, L. G. (2012) The role of pH and Mg on the stability and crystallization of amorphous calcium carbonate. *J. Alloys Compounds* **536,** S477–S479 CrossRef
94. Gong, Y. U. T., Killian, C. E., Olson, I. C., Appathurai, N. P., Amasino, A. L., Martin, M. C., Holt, L. J., Wilt, F. H., and Gilbert, P. U. P. A. (2012) Phase transitions in biogenic amorphous calcium carbonate. *Proc. Natl. Acad. Sci. U.S.A.* **109,** 6088–6093 CrossRef Medline
95. Falini, G., Fermani, S., and Goffredo, S. (2015) Coral biomineralization: a focus on intra-skeletal organic matrix and calcification. *Semin. Cell Dev. Biol.* **46,** 17–26 CrossRef Medline
96. Politi, Y., Mahamid, J., Goldberg, H., Weiner, S., and Addadi, L. (2007) Asprich mollusk shell protein: *in vitro* experiments aimed at elucidating function in CaCO3 crystallization. *Crystengcomm* **9,** 1171–1177 CrossRef
97. Mikšík, I., Eckhardt, A., Sedláková, P., and Mikulikova, K. (2007) Proteins of insoluble matrix of avian (*Gallus gallus*) eggshell. *Connect Tissue Res.* **48,** 8 CrossRef
98. Dombre, C., Guyot, N., Moreau, T., Monget, P., Da Silva, M., Gautron, J., and Réhault-Godbert, S. (2017) Egg serpins: the chicken and/or the egg dilemma. *Semin. Cell Dev. Biol.* **62,** 120–132 CrossRef Medline
99. Hincke, M. T., Gautron, J., Panheleux, M., Garcia-Ruiz, J., McKee, M. D., and Nys, Y. (2000) Identification and localization of lysozyme as a component of eggshell membranes and eggshell matrix. *Matrix Biol.* **19,** 443–453 CrossRef
100. Voinescu, A. E., Touraud, D., Lecker, A., Pfitzner, A., Kunz, W., and Ninham, B. W. (2007) Mineralization of CaCO3 in the presence of egg white lysozyme. *Langmuir* **23,** 12269–12274 CrossRef Medline
101. Wang, X. Q., Sun, H. L., Xia, Y. Q., Chen, C. X., Xu, H., Shan, H. H., and Lu, J. R. (2009) Lysozyme mediated calcium carbonate mineralization. *J. Colloid Interface Sci.* **332,** 96–103 CrossRef Medline
102. Hincke, M. T. (1995) Ovalbumin is a component of the chicken eggshell matrix. *Connect. Tissue Res.* **31,** 227–233 CrossRef Medline
103. Pipich, V., Balz, M., Wolf, S. E., Tremel, W., and Schwahn, D. (2008) Nucleation and growth of CaCO3 mediated by the egg-white protein ovalbumin: a time-resolved *in situ* study using small-angle neutron scattering. *J. Am. Chem. Soc.* **130,** 6879–6892 CrossRef Medline
104. Schwahn, D., Balz, M., and Tremel, W. (2004) Crystallization of the $CaCO_3$ mineral in the presence of the protein ovalbumin. *Physica B Condensed Matter* **350,** E947–E949 CrossRef
105. Wang, X. Q., Wu, C. M., Tao, K., Zhao, K., Wang, J. Q., Xu, H., Xia, D. H., Shan, H. H., and Lu, J. R. (2010) Influence of ovalbumin on $CaCO_3$ precipitation during *in vitro* biomineralization. *J. Phys. Chem. B* **114,** 5301–5308 CrossRef Medline
106. Wang, X., Kong, R., Pan, X., Xu, H., Xia, D., Shan, H., and Lu, J. R. (2009) Role of ovalbumin in the stabilization of metastable vaterite in calcium carbonate biomineralization. *J. Phys. Chem. B* **113,** 8975–8982 CrossRef Medline
107. Gautron, J., Hincke, M. T., Panheleux, M., Garcia-Ruiz, J. M., Boldicke, T., and Nys, Y. (2001) Ovotransferrin is a matrix protein of the hen eggshell membranes and basal calcified layer. *Connect. Tissue Res.* **42,** 255–267 CrossRef Medline
108. Mann, K., and Mann, M. (2008) The chicken egg yolk plasma and granule proteomes. *Proteomics* **8,** 178–191 CrossRef Medline
109. Guérin-Dubiard, C., Anton, M., Gautron, J., Nys, Y., and Nau, F. (2010) Composition de l'oeuf. In *Science et technologie de l'oeuf* (Nau, F., Guérin-Dubiard, C., Baron, F., and Thapon, J. L., eds) pp. 1–169, Lavoisier, Cachan
110. Mann, K., Gautron, J., Nys, Y., McKee, M. D., Bajari, T., Schneider, W. J., and Hincke, M. I. (2003) Disulfide-linked heterodimeric clusterin is a component of the chicken eggshell matrix and egg white. *Matrix Biol.* **22,** 397–407 CrossRef Medline
111. Gautron, J., and Nys, Y. (2007) Eggshell matrix proteins. In *Bioactive Egg Compounds* (Huopalahti, R., López-Fandiño, R., Anton, M., and Schade, R., eds) pp. 103–108, Springer, Berlin
112. Théry, C., Amigorena, S., Raposo, G., and Clayton, A. (2006) Isolation and characterization of exosomes from cell culture supernatants and biological fluids. *Curr. Protocols Cell Biol.* **30,** 3.22.1–3.22.29 CrossRef
113. Wu, L. N., Genge, B. R., Sauer, G. R., and Wuthier, R. E. (1996) Characterization and reconstitution of the nucleational complex responsible for mineral formation by growth plate cartilage matrix vesicles. *Connect. Tissue Res.* **35,** 309–315 CrossRef Medline
114. Kirsch, T., and Claassen, H. (2000) Matrix vesicles mediate mineralization of human thyroid cartilage. *Calcif. Tissue Int.* **66,** 292–297 CrossRef Medline
115. Kirsch, T., Harrison, G., Golub, E. E., and Nah, H. D. (2000) The roles of annexins and types II and X collagen in matrix vesicle-mediated mineralization of growth plate cartilage. *J. Biol. Chem.* **275,** 35577–35583 CrossRef Medline
116. Kapustin, A. N., Davies, J. D., Reynolds, J. L., McNair, R., Jones, G. T., Sidibe, A., Schurgers, L. J., Skepper, J. N., Proudfoot, D., Mayr, M., and Shanahan, C. M. (2011) Calcium regulates key components of vascular smooth muscle cell-derived matrix vesicles to enhance mineralization. *Circ. Res.* **109,** e1–e12 CrossRef Medline
117. Cui, L., Houston, D. A., Farquharson, C., and MacRae, V. E. (2016) Characterisation of matrix vesicles in skeletal and soft tissue mineralisation. *Bone* **87,** 147–158 CrossRef Medline
118. Davies, O. G., Cox, S. C., Williams, R. L., Tsaroucha, D., Dorrepaal, R. M., Lewis, M. P., and Grover, L. M. (2017) Annexin-enriched osteoblast-derived vesicles act as an extracellular site of mineral nucleation within developing stem cell cultures. *Sci. Rep.* **7** CrossRef
119. Yang, K. T., Lin, C. Y., Liou, J. S., Fan, Y. H., Chiou, S. H., Huang, C. W., Wu, C. P., Lin, E. C., Chen, C. F., Lee, Y. P., Lee, W. C., Ding, S. T., Cheng, W. T. K., and Huang, M. C. (2007) Differentially expressed transcripts in shell glands from low and high egg production strains of chickens using cDNA microarrays. *Anim. Reprod. Sci.* **101,** 113–124 CrossRef Medline